J|A|C|S
ARTICLES
Published on Web 03/16/2007

A Class of Luminescent Cyclometalated Alkynylgold(III) Complexes: Synthesis, Characterization, and Electrochemical, Photophysical, and Computational Studies of [Au(C^N^C)(C≡C−R)] (C^N^C = κ^3C,N,C Bis-cyclometalated 2,6-Diphenylpyridyl)

Keith Man-Chung Wong, Ling-Ling Hung, Wai Han Lam, Nianyong Zhu, and Vivian Wing-Wah Yam*

Contribution from the Centre for Carbon-Rich Molecular and Nano-Scale Metal-Based Materials Research and Department of Chemistry, The University of Hong Kong, Pokfulam Road, Hong Kong

Received November 18, 2006; E-mail: wwyam@hku.hk

Abstract: A new class of luminescent cyclometalated alkynylgold(III) complexes, [Au(RC^N(R′)^CR)(C≡CR″)], i.e., [Au(C^N^C)(C≡CR″)] (HC^N^CH = 2,6-diphenylpyridine) R″ = C_6H_5 **1**, C_6H_4−Cl-*p* **2**, C_6H_4−NO_2-*p* **3**, C_6H_4−OCH_3-*p* **4**, C_6H_4−NH_2-*p* **5**, C_6H_4−C_6H_{13}-*p* **6**, C_6H_{13} **7**, [Au(^{t}BuC^N^C^{t}Bu)(C≡CC_6H_5)] **8** (H^tBuC^N^C^{t}BuH = 2,6-bis(4-*tert*-butylphenyl)pyridine), and [Au(C^NTol^C)(C≡CC_6H_4−C_6H_{13}-*p*)] **9** (HC^NTol^CH = 2,6-diphenyl-4-*p*-tolylpyridine), have been synthesized and characterized. The X-ray crystal structures of most of the complexes have also been determined. Electrochemical studies show that, in general, the first oxidation wave is an alkynyl ligand-centered oxidation, while the first reduction couple is ascribed to a ligand-centered reduction of the cyclometalated ligand with the exception of **3** in which the first reduction couple is assigned as an alkynyl ligand-centered reduction. Their electronic absorption and luminescence behaviors have also been investigated. In dichloromethane solution at room temperature, the low-energy absorption bands are assigned as the $\pi-\pi^*$ intraligand (IL) transition of the cyclometalated RC^N(R′)^CR ligand with some mixing of a [π(C≡CR″) → π^*(RC^N(R′)^CR)] ligand-to-ligand charge transfer (LLCT) character. The low-energy emission bands of all the complexes, with the exception of **5**, are ascribed to origins mainly derived from the $\pi-\pi^*$ IL transition of the cyclometalated RC^N(R′)^CR ligand. In the case of **5** that contains an electron-rich amino substituent on the alkynyl ligand, the low-energy emission band was found to show an obvious shift to the red. A change in the origin of emission is evident, and the emission of **5** is tentatively ascribed to a [π(C≡C$C_6H_4NH_2$) → π^*(C^N^C)] LLCT excited-state origin. DFT and TDDFT computational studies have been performed to verify and elucidate the results of the electrochemical and photophysical studies.

Introduction

The common oxidation states of gold are found for +1 and +3, with other oxidation states such as +2, +4, and +5 being much less common. The chemistry of gold(I) has attracted a great amount of attention; in particular there has been a recent revival of interest in light of the observation of weak inter- or intramolecular gold···gold interactions in a number of mono- and polynuclear gold(I) complexes.[1] Studies of gold(I) complexes have further been promoted by the recent reports on the rich and interesting photophysical and photochemical properties displayed by a number of gold(I) complexes.[2,3] Among the gold(I) complexes, gold(I) alkynyls represent an interesting class of organogold compounds, with its growing interest partly stemming from the recent reports on its rich luminescence properties[3] and the ability of gold(I) and alkynyl moieties to build supramolecular architectures based on the tendency of gold(I) to form two-coordinate linear geometry and aurophilic interactions,[4] and the tendency of alkynyl units to function as linear rigid-rod building blocks.

(1) (a) Schmidbaur, H.; Cronje, S.; Djordjevic, B.; Schuster, O. *Chem. Phys.* **2005**, *311*, 151. (b) Schmidbaur, H. *Chem. Soc. Rev.* **1995**, *24*, 391. (c) Pyykkö, P. *Chem. Rev.* **1988**, *88*, 563.

(2) (a) Yam, V. W. W.; Lo, K. K. W. *Chem. Soc. Rev.* **1999**, 323. (b) Ford, P. C.; Vogler, A. *Acc. Chem. Res.* **1993**, *26*, 220. (c) Fung, E. I.; Olmstead, M. M.; Vickery, J. C.; Balch, A. L. *Coord. Chem. Rev.* **1998**, *171*, 151. (d) Burini, A.; Mohamed, A. A.; Fackler, J. P., Jr. *Comments Inorg. Chem.* **2003**, *24*, 253.

(3) (a) Li, D.; Hong, X.; Che, C. M.; Lo, W. C.; Peng, S. M. *J. Chem. Soc., Dalton Trans.* **1993**, 2929. (b) Müller, T. E.; Choi, S. W. K.; Mingos, D. M. P.; Murphy, D.; Williams, D. J.; Yam, V. W. W. *J. Organomet. Chem.* **1994**, *484*, 209. (c) Lu, W.; Xiang, H. F.; Zhu, N.; Che, C. M. *Organometallics* **2002**, *21*, 2343. (d) Che, C. M.; Chao, H. Y.; Miskowski, V. M.; Li, Y.; Cheung, K. K. *J. Am. Chem. Soc.* **2001**, *123*, 4985. (e) Yam, V. W. W.; Choi, S. W. K.; Cheung, K. K. *Organometallics* **1996**, *15*, 1734. (f) Yam, V. W. W.; Choi, S. W. K. *J. Chem. Soc., Dalton Trans.* **1996**, 4227. (g) Lu, X. X.; Li, C. K.; Cheng, E. C. C.; Zhu, N.; Yam, V. W. W. *Inorg. Chem.* **2004**, *43*, 2225. (h) Yam, V. W. W.; Yip, S. K.; Yuan, L. H.; Cheung, K. L.; Zhu, N.; Cheung, K. K. *Organometallics* **2003**, *22*, 2630. (i) Yip, S. K.; Cheng, E. C. C.; Zhu, N.; Yam, V. W. W. *Angew. Chem., Int. Ed.* **2004**, *43*, 4954. (j) Yam, V. W. W.; Lo, K. K. W.; Wong, K. M. C. *J. Organomet. Chem.* **1999**, *578*, 3.

(4) (a) Mingos, D. M. P.; Yau, J.; Menzer, S.; Williams, D. J. *Angew. Chem., Int. Ed.* **1995**, *34*, 1894. (b) McArdle, C. P.; Irwin, M. J.; Jennings, M. C.; Vittal, J. J.; Puddephatt, R. J. *Chem.—Eur. J.* **2002**, *8*, 723.

10.1021/ja068264u CCC: $37.00

Gold(III) complexes are mainly dominated by complexation with nitrogen- or oxygen-donor ligands and halide ligands,[5] though gold(III) complexes of phosphines and thiolates have also been reported, mainly in the form of alkyls, aryls, and ylides.[5] In contrast to the gold(I) system, gold(III) complexes have been rarely observed to emit, and even if they emit, they usually would do so at low temperature in the solid state or in low-temperature glasses, with very few examples that would emit at room temperature in solution.[6] Probable reason for the lack of luminescence behavior in gold(III) species is the presence of low-energy d−d ligand field (LF) states. The presence of a nonemissive low-lying d−d state would quench the luminescence excited state via thermal equilibration or energy transfer.[6a] Despite a number of organogold(III) complexes reported,[5] most of them are relatively unstable and readily undergo reductive elimination reactions to give carbon−carbon coupling products and gold(I) species, especially in the presence of light. As a consequence, luminescence studies of organogold(III) complexes and related studies on luminescent gold(III) systems are scarce[6] in spite of the fact that the related gold(I) and the isoelectronic platinum(II) analogues are known to be strongly emissive. Examples of luminescent organogold(III) compounds include certain classes of gold(III) aryl compounds[6b] and cyclometalated gold(III) compounds[6c−e,7] which are rather stable, even upon visible light irradiation, with interesting luminescence properties.[6c−e,7] The first examples of luminescent organogold(III) complexes were reported by us in 1993, in which the luminescence behavior of a novel series of stable diaryl- and dialkylgold(III) diimine complexes, $[Au(N\hat{}N)R_2]^+$ (N^N = bpy, phen; R = CH_2SiMe_3, mesityl), were described.[6b] These complexes were found to show rich luminescence behavior both in the solid state and in solution at 298 and 77 K. We envisaged that introduction of strong σ-donating alkynyls to gold(III) would render the metal center more electron-rich, with the additional advantage of raising the energy of the d−d states, resulting in an improvement or enhancement of the luminescence by

Chart 1

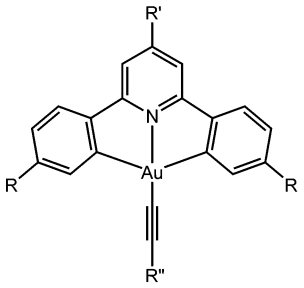

R and R' = H; R" =	
C_6H_5	(**1**)
C_6H_4–Cl-*p*	(**2**)
C_6H_4–NO_2-*p*	(**3**)
C_6H_4–OCH_3-*p*	(**4**)
C_6H_4–NH_2-*p*	(**5**)
C_6H_4–C_6H_{13}-*p*	(**6**)
C_6H_{13}	(**7**)

R = ^{t}Bu; R' = H; R" =	
C_6H_5	(**8**)

R = H; R' = C_6H_4-CH_3-*p*; R" =	
C_6H_4–C_6H_{13}-*p*	(**9**)

increasing the chances for population of the emissive state. However, while alkynyl complexes of gold(I)[3] and the isoelectronic platinum(II)[3j,8,9] are known and shown to display rich photoluminescence properties, the chemistry of alkynylgold(III) is essentially rare[10] despite the fact that there is increasing interest in the use of gold(III) compounds for catalysis of organic synthetic reactions of alkynes,[11] and their luminescence behavior is virtually unknown. The alkynyl group, with the inherent rigidity of its structure, its ability to interact with metal centers via pπ-dπ overlap which can effectively strengthen the metal−carbon bonds, and its extended π-electron delocalization, is an ideal candidate for the construction of luminescent organometallic materials. Moreover, the introduction of heavy gold metal centers into the alkynyl backbone in metal-containing oligo- and poly-ynes would also provide a versatile method to improve the chances of producing triplet emitters, leading to long-lived triplet emission, as a result of a larger spin−orbit coupling constant and an enhanced intersystem crossing efficiency.

We recently communicated the synthesis and rich luminescence properties of a novel class of luminescent alkynylgold(III) complexes, [Au(C^N^C)(C≡C−R)] (HC^N^CH = 2,6-diphenylpyridine).[7] These complexes represent isoelectronic and structural analogues of interesting classes of alkynyl platinum(II) terpyridyl,[9] $[Pt(N\hat{}N\hat{}N)(C{\equiv}CR)]^+$, and cyclometalated, [Pt(C^N^N)(C≡CR)], complexes[8i] that also exhibit interesting and affluent photophysical behaviors. As an extension of our previous studies, together with our great interest in transition metal alkynyl complexes,[9,12] we report herein the synthesis, characterization, electrochemical, and photophysical studies of a series of luminescent alkynylgold(III) complexes with various cyclometalated and alkynyl ligands, [Au(RC^N(R′)^CR)(C≡CR″)], i.e., [Au(C^N^C)(C≡CR″)] (HC^N^CH = 2,6-diphenylpyridine) R″ = C_6H_5 **1**, C_6H_4−Cl-*p* **2**, C_6H_4−NO_2-*p* **3**, C_6H_4−OCH_3-*p* **4**, C_6H_4−NH_2-*p* **5**, C_6H_4−C_6H_{13}-*p* **6**, C_6H_{13} **7**, [Au(^{t}BuC^N^C^{t}Bu)(C≡CC_6H_5)] **8** (H^{t}BuC^N^C^{t}BuH = 2,6-bis(4-*tert*-butylphenyl)pyridine), and [Au(C^NTol^C)(C≡CC_6H_4−

(5) Grohmann, A.; Schmidbaur, H. *Comprehensive Organometallic Chemistry II*; Abel, E. W., Stone, F. G. A., Wilkinson, G., Eds.; Pergamon: Oxford, New York, 1995; Vol. 3, Chapter 1.
(6) (a) Vogler, A.; Kunkely, H. *Coord. Chem. Rev.* **2001**, *219*−*221*, 489. (b) Yam, V.W.W.; Choi, S. W. K.; Lai, T. F.; Lee, W. K. *J. Chem. Soc., Dalton Trans.* **1993**, 1001. (c) Chan, C. W.; Wong, W. T.; Che, C. M. *Inorg. Chem.* **1994**, *33*, 1266. (d) Wong, K. H.; Cheung, K. K.; Chan, M. C. W.; Che, C. M. *Organometallics* **1998**, *17*, 3505. (e) Mansour, M. A.; Lachicotte, R. J.; Gysling, H. J.; Eisenberg, R. *Inorg. Chem.* **1998**, *37*, 4625.
(7) (a) Yam, V. W. W.; Wong, K. M. C.; Hung, L. L.; Zhu, N. *Angew. Chem., Int. Ed.* **2005**, *44*, 3107. (b) Wong, K. M. C.; Zhu, X.; Hung, L. L.; Zhu, N.; Yam, V. W. W.; Kwok, H. S. *Chem. Commun.* **2005**, 2906.
(8) (a) Sacksteder, L.; Baralt, E.; DeGraff, B. A.; Lukehart, C. M.; Demas, J. N. *Inorg. Chem.* **1991**, *30*, 2468. (b) Lewis, J.; Khan, M. S.; Kakkar, A. K.; Johnson, B. F. G.; Marder, T. B.; Fyfe, H. B.; Wittmann, F.; Friend, R. H.; Dray, A. E. *J. Organomet. Chem.* **1992**, *425*, 165. (c) Wittmann, H. F.; Friend, R. H.; Khan, M. S.; Lewis, J. *J. Chem. Phys.* **1994**, *101*, 2694. (d) Liu, Y.; Jiang, S.; Glusac, K.; Powell, D. H.; Anderson, D. F.; Schanze, K. S. *J. Am. Chem. Soc.* **2002**, *124*, 12412. (e) Chan, C. W.; Cheng, L. K.; Che, C. M. *Coord. Chem. Rev.* **1994**, *132*, 87. (f) Hissler, M.; William, B. C.; Geiger, D. K.; McGarrah, D. L.; Lachicotte, R. J.; Eisenberg, R. *Inorg. Chem.* **2000**, *39*, 447. (g) Whittle, C. E.; Weinstein, J. A.; George, M. W.; Schanze, K.S. *Inorg. Chem.* **2001**, *40*, 4053. (h) James, S. L.; Younus, M.; Raithby, P. R.; Lewis, J. *J. Organomet. Chem.* **1997**, *543*, 233. (i) Lu, W.; Mi, B. X.; Chan, M. C. W.; Hui, Z.; Che, C. M.; Zhu, N.; Lee, S. T. *J. Am. Chem. Soc.* **2004**, *126*, 4958.
(9) (a) Yam, V. W. W.; Tang, R. P. L.; Wong, K. M. C.; Cheung, K. K. *Organometallics* **2001**, *20*, 4476. (b) Yam, V. W. W.; Wong, K. M. C.; Zhu, N. *J. Am. Chem. Soc.* **2002**, *124*, 6506. (c) Yam, V. W. W.; Wong, K. M. C.; Zhu, N. *Angew. Chem., Int. Ed.* **2003**, *42*, 1400. (d) Yam, V. W. W.; Chan, K. H. Y.; Wong, K. M. C.; Zhu, N. *Chem.—Eur. J.* **2005**, *11*, 4535. (e) Wong, K. M. C.; Tang, W. S.; Chu, B. W. K.; Zhu, N.; Yam, V. W. W. *Organometallics* **2004**, *23*, 3459. (f) Wong, K. M. C.; Tang, W. S.; Lu, X. X.; Zhu, N.; Yam, V. W. W. *Inorg. Chem.* **2005**, *44*, 1492. (h) Tang, W. S.; Lu, X. X.; Wong, K. M. C.; Yam, V. W. W. *J. Mater. Chem.* **2005**, *15*, 2714.
(10) (a) Johnson, A.; Puddephatt, R. J. *J. Chem. Soc., Dalton Trans.* **1977**, 1384. (b) Cinellu, M. A.; Minghetti, G.; Pinna, M. V.; Stoccoro, S.; Zucca, A.; Manassero, M. *J. Chem. Soc., Dalton Trans.* **1999**, 2823. (c) Méndez, L. A.; Jiménez, J.; Cerrada, E.; Mohr, F.; Laguna, M. *J. Am. Chem. Soc.* **2005**, *127*, 852. (d) Schuster, O.; Schmidbaur, H. *Organometallics* **2005**, *24*, 2289.
(11) (a) Asao, N.; Nogami, T.; Lee, S.; Yamamoto, Y. *J. Am. Chem. Soc.* **2003**, *125*, 10921. (b) Hashmi, A. S. K. *Gold Bull.* **2003**, *36*, 3.
(12) (a) Yam, V. W. W. *Chem. Commun.* **2001**, 789. (b) Yam, V. W. W. *Acc. Chem. Res.* **2002**, *35*, 555. (c) Lo, W. Y; Lam, C. H.; Yam, V. W. W.; Zhu, N.; Cheung, K. K.; Fathallah, S.; Messaoudi, S.; Guennic, B. L.; Kahlal, S.; Halet, J. F. *J. Am. Chem. Soc.* **2004**, *126*, 7300. (d) Yam, V. W. W.; Lo, K. K. W. *Chem. Soc. Rev.* **1999**, *28*, 323. (e) Yam, V. W. W.; Fung, W. K. M.; Cheung, K. K. *Angew. Chem., Int. Ed.* **1996**, *35*, 1100. (f) Yam, V. W. W.; Lo, W. Y; Zhu, N. *Chem. Commun.* **1997**, 963.

Scheme 1

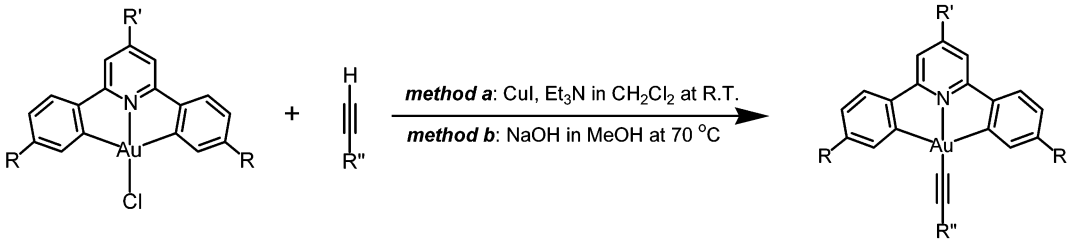

C_6H_{13}-*p*)] **9** (HC^NTol^CH = 2,6-diphenyl-4-*p*-tolylpyridine) (Chart 1); DFT and TDDFT computational studies have also been performed to elucidate the electronic structures of the complexes and the nature of their excited states.

Results and Discussion

Synthesis and Characterization. The incorporation of alkynyl ligand into the cyclometalated gold(III) moiety, [Au(RC^N(R′)^CR)], was achieved by two methodologies (Scheme 1). In *method a*, a reaction mixture of the chlorogold(III) precursor, alkyne, triethylamine, and a catalytic amount of copper(I) iodide was allowed to stir for 3 h at room temperature in dichloromethane under a nitrogen atmosphere to give the corresponding alkynylgold(III) complex. In *method b*, the preparation of the desired alkynylgold(III) complex was accomplished by heating a methanolic solution of the chlorogold(III) precursor, alkyne, and sodium hydroxide at 70 °C for 12 h under a nitrogen atmosphere. In both cases, pale yellow crude products were obtained by evaporation of the solvent to dryness, which were then purified by column chromatography on silica gel using dichloromethane as eluent. Subsequent recrystallization from slow diffusion of diethyl ether vapor into the concentrated solution of the complex resulted in the isolation of the desired product as pale yellow crystals. In view of the higher product yield obtained from *method a* (68−88%) than that from *method b* (ca. 40%) as well as the shorter reaction time required, *method a* was the method of choice for the synthesis of the target alkynylgold(III) complexes. All the complexes are found to be air-stable and thermal-stable. The incorporation of alkynyl ligand into the gold(III) center renders the products more soluble in common organic solvents, especially relative to the precursor complex, [Au(C^N^C)Cl], which is only soluble in DMSO. The identities of complexes **1**−**9** have been confirmed by ^{1}H NMR spectroscopy, EI- or FAB-mass spectrometry, IR spectroscopy, and satisfactory elemental analyses. The IR spectra of the complexes show a weak band at 2143−2157 cm^{-1}, typical of the ν(C≡C) stretching frequency. The crystal structures of all the complexes (with the exception of **6**) have also been determined by X-ray crystallography.

X-ray Crystal Structures. Single crystals of **1**−**5** and **7**−**9** were obtained by slow diffusion of diethyl ether vapor into a dichloromethane solution of the respective complexes or by layering of *n*-hexane onto a concentrated dichloromethane solution of the complexes, and their structures were solved by X-ray crystallography. Crystal structure determination data are summarized in Table 1. The selected bond distances and bond angles as well as selected intermolecular parameters are tabulated in Tables 2 and 3, respectively. The structure of **1** has been previously communicated.[7a] The representative perspective views of the crystal structures are depicted in Figure 1. In each case, the gold(III) metal center coordinates to the bis-cyclometalated tridentate RC^N(R′)^CR pincer ligand with the remaining site occupied by an alkynyl ligand to give a distorted square-planar geometry, characteristic of d^8 metal complexes. The C−Au−C and C−Au−N angles of 161.1(4)°−164.1(9)° and 79.9°−82.6° about the gold(III) metal center deviate from the idealized values of 180° and 90°, respectively, due to the restricted bite angle of the tridentate ligand. The [Au(RC^N(R′)^CR)] motif is essentially coplanar, and the Au−C (2.047−2.084 Å) and Au−N (1.999−2.039 Å) bond distances are similar to those found in other related bis-cyclometalated gold(III) complexes.[6d] The Au−C≡C angles range from 171.6° to 180°, establishing a slightly distorted linear arrangement, with the Au−C (1.945−2.008 Å) bond parameter similar to those found in the other alkynylgold(III) system,[10c,d] while the C≡C bond distances (1.124−1.220 Å) are in the range typical of transition metal alkynyl systems.[3a,c−i,8e−i,9a−f,10c,d,11c,e,f] The interplanar angles between the phenyl ring of the alkynyl ligand and the [Au(RC^N(R′)^CR)] plane in complexes **1**−**5**, **8**, and **9** vary from 16.3° to 88.9°, while that in the two independent molecules of **5** are 49.4° and 74.0° (Table 3). It is likely that the energy barrier for the rotation of the phenyl ring relative to the [Au(RC^N(R′)^CR)] plane should be very low so that there is no preference for the coplanar or orthogonal orientation of the phenyl ring with respect to the [Au(RC^N(R′)^CR)] plane. However, crystal packing forces may exert an influence on the ultimate orientation of the phenyl ring relative to that of the [Au(RC^N(R′)^CR)] plane.

Although the closest Au···Au distances (3.846−5.951 Å) between adjacent molecules are found to be longer than the sum of van der Waals radii for two gold(III) centers, suggestive of insignificant Au···Au contacts in their crystal lattices, the shortest interplanar distances between the [Au(RC^N(R′)^CR)] planes are found to range from 3.4 to 3.6 Å (Table 3), indicating the presence of appreciable $\pi-\pi$ stacking interactions as revealed by their crystal packings for many of the structures. It is interesting to note that their packing arrangements vary from one structure to another. For crystals of **1**, **3**, **4**, and **8**, the complex molecules are stacked into an extended columnar array with identical Au···Au and $\pi-\pi$ separations between them, while the [Au(RC^N(R′)^CR)] motifs are partially stacked with different extents of aromatic overlapping (Figure 2a−d). The [Au(RC^N(R′)^CR)] moieties are stacked in a variety of manners (head-to-tail in **1**; head-to-head in **3**; partial head-to-tail in **4**) and are shifted laterally with respect to each other, while the crystal packing of **8** shows that the molecules are arranged in a head-to-tail fashion without a lateral shift of the [Au(RC^N(R′)^CR)] units, probably resulting from the minimization of the mutual repulsion between the sterically bulky *tert*-butyl groups (Figure 2e). With **2**, **5**, **7**, and **9**, the molecules

Table 1. Crystal and Structure Determination Data of **1**−**5** and **7**−**9**

complex	**1**	**2**	**3**	**4**·$^1/_2$ *n*-hexane	**5**	**7**	**8**	**9**·CH_2Cl_2
empirical formula	$C_{25}H_{16}AuN$	$C_{25}H_{15}AuClN$	$C_{25}H_{15}AuN_2O_2$	$C_{29}H_{25}AuNO$	$C_{25}H_{17}AuN_2$	$C_{25}H_{24}AuN$	$C_{33}H_{32}AuN$	$C_{39}H_{36}AuCl_2N$
formula weight	527.35	561.80	572.36	600.47	542.37	535.42	639.56	786.55
temp, K	253(2)	301(2)	253(2)	253(2)	243(2)	253(2)	301(2)	253(2)
wavelength, Å	0.710 73	0.710 73	0.710 73	0.710 73	0.710 73	0.710 73	0.710 73	0.710 73
crystal system	orthorhombic	triclinic	monoclinic	monoclinic	triclinic	triclinic	monoclinic	monoclinic
space group	$P2_12_12_1$	$P\bar{1}$	$P2_1/c$	$P2_1/c$	$P\bar{1}$	$P\bar{1}$	$C2/c$	$P2_1/n$
a, Å	6.735(1)	7.4590(15)	5.100	12.934(3)	11.156(2)	8.282(2)	19.335(4)	8.637(2)
b, Å	14.265(3)	9.6410(19)	15.197(3)	19.404(4)	12.539(3)	9.029(2)	19.732(4)	20.419(4)
c, Å	19.583(4)	14.086(3)	25.241(5)	9.697(2)	14.737(3)	13.870(3)	7.172(1)	18.930(4)
α, deg	90	106.07(3)	90	90	80.73(3)	84.67(3)	90	90
β, deg	90	97.74(3)	95.58(3)	107.33(3)	70.56(3)	81.18(3)	99.76(3)	101.81(3)
γ, deg	90	94.98(3)	90	90	79.77(3)	84.33(3)	90	90
volume, cm^3	1881.4(6)	956.3(3)	1947.0(7)	2323.2(8)	1901.5(7)	1016.7(4)	2696.6(9)	3267.8(11)
Z, $Å^3$	4	2	4	4	4	2	4	4
density (calcd), g cm^{-3}	1.862	1.951	1.953	1.717	1.895	1.749	1.575	1.599
crystal size, mm^3	0.4 × 0.2 × 0.2	0.60 × 0.20 × 0.12	0.3 × 0.15 × 0.08	0.4 × 0.08 × 0.04	0.4 × 0.25 × 0.1	0.5 × 0.4 × 0.2	0.5 × 0.3 × 0.25	0.4 × 0.25 × 0.2
index ranges	$-7 \le h \le 7$ $-17 \le k \le 17$ $-23 \le l \le 23$	$-8 \le h \le 8$ $-11 \le k \le 11$ $-16 \le l \le 16$	$-5 \le h \le 5$ $-17 \le k \le 17$ $-25 \le l \le 26$	$-11 \le h \le 11$ $-18 \le k \le 18$ $-9 \le l \le 9$	$-13 \le h \le 13$ $-15 \le k \le 15$ $-17 \le l \le 17$	$-9 \le h \le 9$ $-10 \le k \le 10$ $-16 \le l \le 15$	$-21 \le h \le 21$ $-23 \le k \le 23$ $-7 \le l \le 7$	$-10 \le h \le 10$ $-24 \le k \le 24$ $-22 \le l \le 22$
reflections collected/unique	10500/3283	6885/3260	6962/2432	5419/1894	11979/6372	5744/3299	8818/2286	24194/6106
GOF on F^2	0.925	1.022	0.915	0.881	0.991	1.054	0.901	1.150
final *R* indices[a] [$I > 2\sigma(I)$]	$R_1 = 0.0262$ $wR_2 = 0.0555$	$R_1 = 0.0386$ $wR_2 = 0.0938$	$R_1 = 0.0366$ $wR_2 = 0.0855$	$R_1 = 0.0514$ $wR_2 = 0.1149$	$R_1 = 0.0516$ $wR_2 = 0.1314$	$R_1 = 0.0500$ $wR_2 = 0.1276$	$R_1 = 0.0262$ $wR_2 = 0.0558$	$R_1 = 0.0298$ $wR_2 = 0.0925$
largest diff peak and hole, e $Å^{-3}$	0.650 and −1.556	1.764 and −2.862	0.550 and −1.482	1.184 and −0.575	2.461 and −3.903	2.311 and −3.313	0.516 and −1.714	0.448 and −1.207

[a] $R_{int} = \sum|F_o^2 - F_o^2\,(\text{mean})|/\sum[F_o^2]$, $R_1 = \sum||F_o| - |F_c||/\sum|F_o|$ and $wR_2 = \{\sum[w(F_o^2 - F_c^2)^2]/\sum[w(F_o^2)^2]\}^{1/2}$.

are stacked together with alternating short and long Au···Au distances to give a "dimeric" configuration. Similar to the extended columnar structures in **1**, **3**, **4**, and **8**, the short Au···Au separations (3.846−5.739 Å) are beyond the range for substantial intermolecular Au···Au interactions. In the "dimeric" unit, the molecules are stacked into pairs with neighboring molecules in a head-to-tail or partial head-to-tail arrangement and are also shifted laterally with respect to each other (Figure 3).

Electrochemistry. In general, the cyclic voltammograms of **1**−**9** in dichloromethane (0.1 mol dm^{-3} $^nBu_4NPF_6$) show one quasi-reversible reduction couple at −1.52 to −1.69 V (vs SCE) and two irreversible oxidation waves in the ranges of +0.76 to +1.68 V and +1.75 to +2.17 V (vs SCE). The electrochemical data are summarized in Table 4, and the representative cyclic voltammograms of **2**, **4**, **7**, and **8** are shown in Figure 4. On the basis of similar potentials observed for the reduction couple in **1**, **2**, and **4**−**6** consisting of the same RC^N(R′)^CR chelate, the reduction process is assigned as the ligand-centered reduction of the RC^N(R′)^CR ligand. The occurrence of this reduction at a more negative potential in **7** (−1.69 V) is also in line with this assignment since the alkyl alkynyl, which is a better *σ*-donor than the aryl alkynyl, would render the gold(III) metal center more electron-rich. As a consequence, the d*π* orbital of the Au(III) center would be higher-lying in energy, causing a destabilization of the *π** orbital of the RC^N(R′)^CR ligand, which would render it more difficult to be reduced. Similarly, the electron-rich *tert*-butyl substituents on the RC^N(R′)^CR ligand in **8** would destabilize the *π** orbital, reducing its ease of reduction to give a more negative potential at −1.64 V. On the other hand, the observation of a less negative potential for the reduction couple in **9** (−1.52 V) is attributed to the presence of the lower-lying *π** orbital owing to the increase in extended *π*-conjugation upon introduction of the aryl substituent on the RC^N(R′)^CR ligand. Since the reduction potential for the RC^N(R′)^CR ligand-centered reduction should not be too sensitive to the nature of the alkynyl ligand, the occurrence of the additional reduction wave at −1.08 V in **3** is suggested to be derived from a ligand-centered reduction of the nitrophenyl alkynyl ligand, while the second reduction wave at −1.52 V is assigned as the C^N^C ligand-centered reduction. This has been supported by DFT calculation, in which the LUMO is mainly derived from the *π** orbital localized on the $C{\equiv}CC_6H_4{-}NO_2$ ligand.

In view of the fact that the potentials for the first irreversible anodic waves, which ranged from +0.76 to +1.68 V, are quite sensitive to the nature of the alkynyl ligand, together with the electron-deficient nature and the unlikely redox activity of the gold(III) metal center, the oxidation wave is assigned as the alkynyl ligand-centered oxidation. For **1**−**6** having the same C^N^C ligand, these anodic waves were found to show potentials in the order **5** < **4** < **6** < **1** ≈ **2** < **3**, in line with the electron-donating ability of the alkynyl group: $C{\equiv}CC_6H_4{-}NH_2$ > $C{\equiv}CC_6H_4{-}OMe$ > $C{\equiv}CC_6H_4{-}C_6H_{13}$ > $C{\equiv}CC_6H_5$ ≈ $C{\equiv}CC_6H_4{-}Cl$ > $C{\equiv}CC_6H_4{-}NO_2$. Thus the better the electron-donating ability of the alkynyl group is, the less positive the potential of the alkynyl ligand-centered oxidation is. This is also consistent with the calculated trend of the HOMO energies (vide infra). The resemblance of the potentials for this oxidation process observed for **1** (+1.57 V) and **8** (+1.59 V), which contain the same alkynyl ligand, and the rather insensitive nature of this potential to the nature of the RC^N(R′)^CR ligand further support this assignment. In general, **7** with the alkyl alkynyl was found to show a more positive potential for this oxidation

Table 2. Selected Bond Lengths (Å) and Angles (deg) for **1**−**5** and **7**−**9** with Estimated Standard Deviations (esd's) Given in Parentheses

1		**2**		**3**		**4**·$^1/_2$ *n*-hexane	
			Bond Lengths (Å)				
Au(1)−C(1)	1.979(7)	Au(1)−C(1)	1.945(8)	Au(1)−C(1)	1.974(10)	Au(1)−C(1)	2.008(19)
Au(1)−C(9)	2.073(7)	Au(1)−C(9)	2.076(8)	Au(1)−C(9)	2.086(13)	Au(1)−C(9)	2.061(16)
Au(1)−C(25)	2.071(7)	Au(1)−C(25)	2.084(7)	Au(1)−C(25)	2.057(10)	Au(1)−C(25)	2.065(16)
Au(1)−N(1)	1.999(5)	Au(1)−N(1)	2.003(6)	Au(1)−N(1)	1.989(9)	Au(1)−N(1)	2.039(13)
C(1)−C(2)	1.185(9)	C(1)−C(2)	1.220(11)	C(1)−C(2)	1.195(11)	C(1)−C(2)	1.19(2)
			Bond Angles (deg)				
C(9)−Au(1)−C(25)	162.0(3)	C(9)−Au(1)−C(25)	162.1(3)	C(9)−Au(1)−C(25)	162.7(4)	C(9)−Au(1)−C(25)	162.4(7)
N(1)−Au(1)−C(1)	178.5(3)	N(1)−Au(1)−C(1)	177.9(2)	N(1)−Au(1)−C(1)	178.8(4)	N(1)−Au(1)−C(1)	178.1(6)
Au(1)−C(1)−C(2)	176.6(7)	Au(1)−C(1)−C(2)	172.7(7)	Au(1)−C(1)−C(2)	172.9(8)	Au(1)−C(1)−C(2)	172.9(15)
N(1)−Au(1)−C(9)	81.1(2)	N(1)−Au(1)−C(9)	80.6(3)	N(1)−Au(1)−C(9)	80.9(5)	N(1)−Au(1)−C(9)	97.4(7)
N(1)−Au(1)−C(25)	80.9(2)	N(1)−Au(1)−C(25)	81.5(3)	N(1)−Au(1)−C(25)	81.8(4)	N(1)−Au(1)−C(25)	81.1(6)
C(1)−C(2)−C(3)	177.6(9)	C(1)−C(2)−C(3)	175.8(8)	C(1)−C(2)−C(3)	177.8(10)	C(1)−C(2)−C(3)	177.2(19)

5		**7**		**8**		**9**·CH_2Cl_2	
			Bond Lengths (Å)				
Au(1)−C(1)	2.008(11)	Au(1)−C(1)	1.980(10)	Au(1)−C(1)	1.972(6)	Au(1)−C(1)	1.967(5)
Au(1)−C(9)	2.078(10)	Au(1)−C(9)	2.078(9)	Au(1)−C(7)	2.065(5)	Au(1)−C(15)	2.073(4)
Au(1)−C(25)	2.064(9)	Au(1)−C(25)	2.045(10)	Au(1)−C(7′)	2.065(5)	Au(1)−C(27)	2.078(5)
Au(1)−N(1)	1.998(7)	Au(1)−N(1)	1.995(7)	Au(1)−N(1)	2.028(5)	Au(1)−N(1)	2.003(3)
C(1)−C(2)	1.118(3)	C(1)−C(2)	1.175(14)	C(1)−C(2)	1.196(8)	C(1)−C(2)	1.191(6)
Au(2)−C(26)	1.998(10)						
Au(2)−C(34)	2.053(11)						
Au(2)−C(50)	2.052(11)						
Au(2)−N(3)	2.014(3)						
C(26)−C(27)	1.126(13)						
			Bond Angles (deg)				
C(9)−Au(1)−C(25)	162.0(4)	C(9)−Au(1)−C(25)	161.1(4)	C(7)−Au(1)−C(7′)	161.9(2)	C(15)−Au(1)−C(27)	162.4(16)
N(1)−Au(1)−C(1)	177.2(3)	N(1)−Au(1)−C(1)	178.2(3)	N(1)−Au(1)−C(1)	180.0	N(1)−Au(1)−C(1)	177.4(17)
Au(1)−C(1)−C(2)	172.7(11)	Au(1)−C(1)−C(2)	171.6(10)	Au(1)−C(1)−C(2)	180.0	Au(1)−C(1)−C(2)	175.0(5)
N(1)−Au(1)−C(9)	81.6(3)	N(1)−Au(1)−C(9)	81.0(3)	N(1)−Au(1)−C(7)	81.0(12)	N(1)−Au(1)−C(15)	81.4(17)
N(1)−Au(1)−C(25)	80.4(3)	N(1)−Au(1)−C(25)	80.1(4)	N(1)−Au(1)−C(7′)	81.0(12)	N(1)−Au(1)−C(27)	81.1(17)
C(1)−C(2)−C(3)	175.4(12)	C(1)−C(2)−C(3)	177.9(13)	C(1)−C(2)−C(3)	180.0(1)	C(1)−C(2)−C(3)	177.6(6)
C(34)−Au(2)−C(50)	162.6(4)						
N(3)−Au(2)−C(26)	177.2(4)						
Au(2)−C(26)−C(27)	175.2(10)						
N(3)−Au(1)−C(34)	81.2(4)						
N(3)−Au(1)−C(50)	81.4(4)						
C(26)−C(27)−C(28)	176.4(12)						

Table 3. Shortest Au···Au Distances and Interplanar Parameters of **1**−**5** and **7**−**9**

complex	shortest Au···Au distances/Å	interplanar angles between [Au(RC^N(R′)^CR)] and phenyl ring of alkynyl/deg	interplanar separations between [Au(RC^N(R′)^CR)] planes[a]/Å	interplanar angles between [Au(RC^N(R′)^CR)] planes/deg
1	5.003	65.0	3.38	2.2
2	4.973	18.1	3.44	0.0
3	5.100	88.9	3.47	0.0
4	5.951	69.8	3.40	0.4
5	3.846	74.0, 49.4	3.53	5.1
7	4.937	−	3.37	0.0
8	4.581	45.6	3.57	0.0
9	5.739	16.3	3.39	0.0

[a] Calculated from the average distances of the atoms on the two least-squares planes.

relative to the others with the aryl alkynyl ligand due to the less π-donating nature of the alkyl alkynyl moiety (see Computational Studies), with the exception of **3** which contains the electron-deficient nitro substituent, rendering the nitrophenyl alkynyl to be the weakest π-donor. For the second oxidation wave, no correlation has been found between their observed potentials and the nature of the ligands, although such an oxidation wave is probably derived from the oxidation of the cyclometallated RC^N(R′)^CR ligand. The lack of a rational trend for this second oxidation potential may be due to the occurrence of decomposition after the first oxidation process on the basis of the fact that a strong anodic signal at −0.7 V, which is typical of electrode adsorption, was observed upon the reduction scan after the first oxidation.

UV−Visible Absorption Spectroscopy. The UV−vis absorption spectra of **1**−**9** in dichloromethane at 298 K feature an intense absorption band at 290−330 nm and a moderately intense vibronic-structured absorption in the 362−415 nm range with extinction coefficients (ϵ) on the order of 10^4 dm^3 mol^{-1} cm^{-1}. The photophysical data of **1**−**9** are summarized in Table 5, and the corresponding electronic absorption spectra of **1**, **3**, **5**, **8**, and **9** are depicted in Figure 5. For complexes **1**−**7**, the absorption energy of the low-energy vibronic band at ca. 400 nm was found to be rather insensitive to the nature of the alkynyl

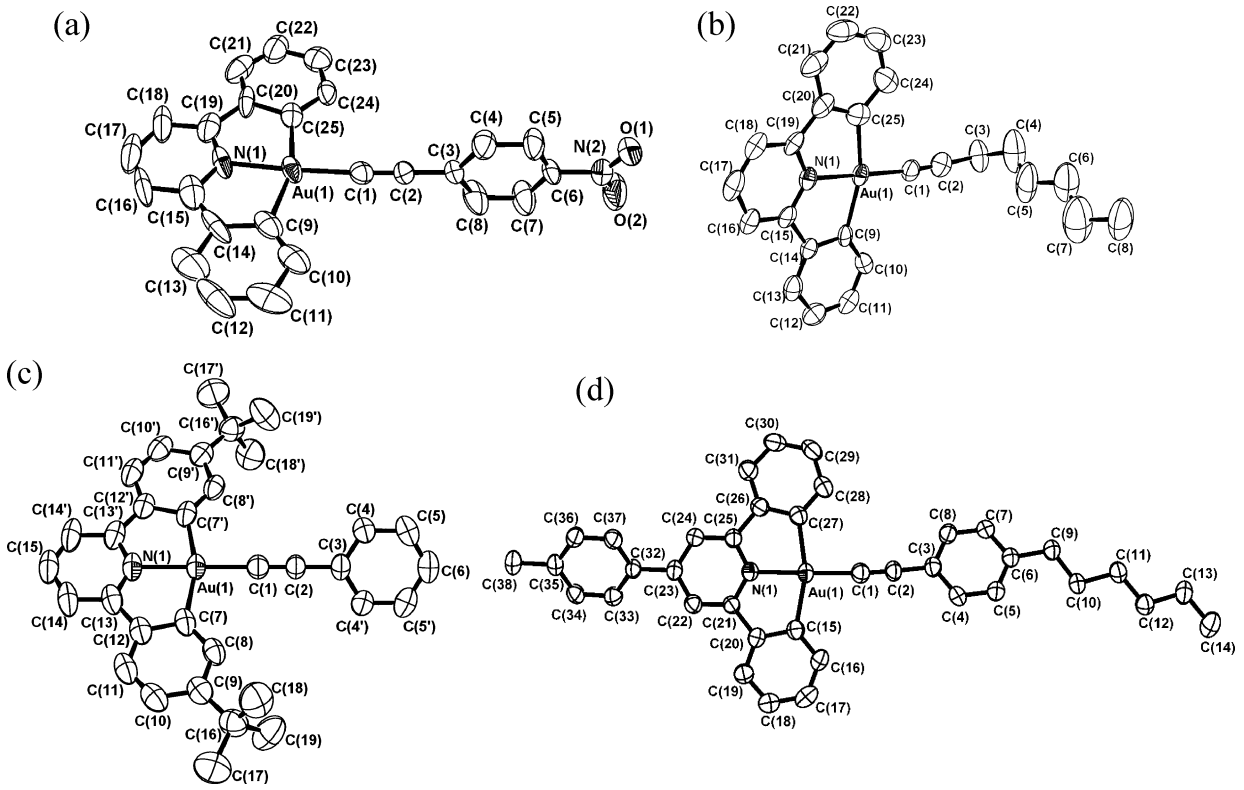

Figure 1. Perspective drawings of **3** (a), **7** (b), **8** (c), and **9** (d) with atomic numbering scheme. Hydrogen atoms and solvent molecules are omitted for clarity. Thermal ellipsoids are drawn at the 50% probability level.

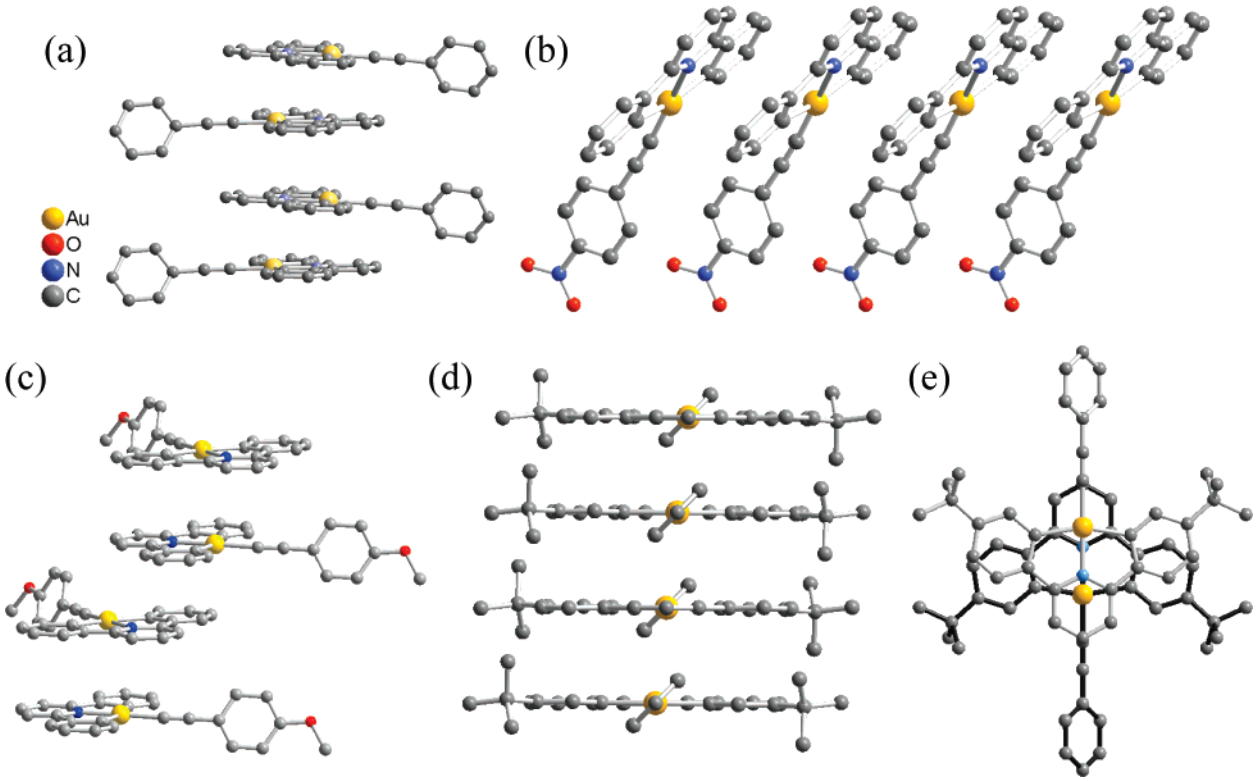

Figure 2. Crystal packing diagrams of **1** (a), **3** (b), **4** (c), and **8** (d) showing an extended columnar array with identical Au···Au and $\pi-\pi$ separations and (e) the head-to-tail configuration of **8**.

ligand. This, together with the observation of vibrational progressional spacings of 1310−1380 cm^{-1} typical of the skeletal vibrational frequency of the RC^N(R′)^CR ligand and the observation of similar absorption band for the chloro counterpart, [Au(C^N^C)Cl] suggested their assignment as a metal-perturbed $\pi \rightarrow \pi^*$ intraligand (IL) transition of the RC^N-

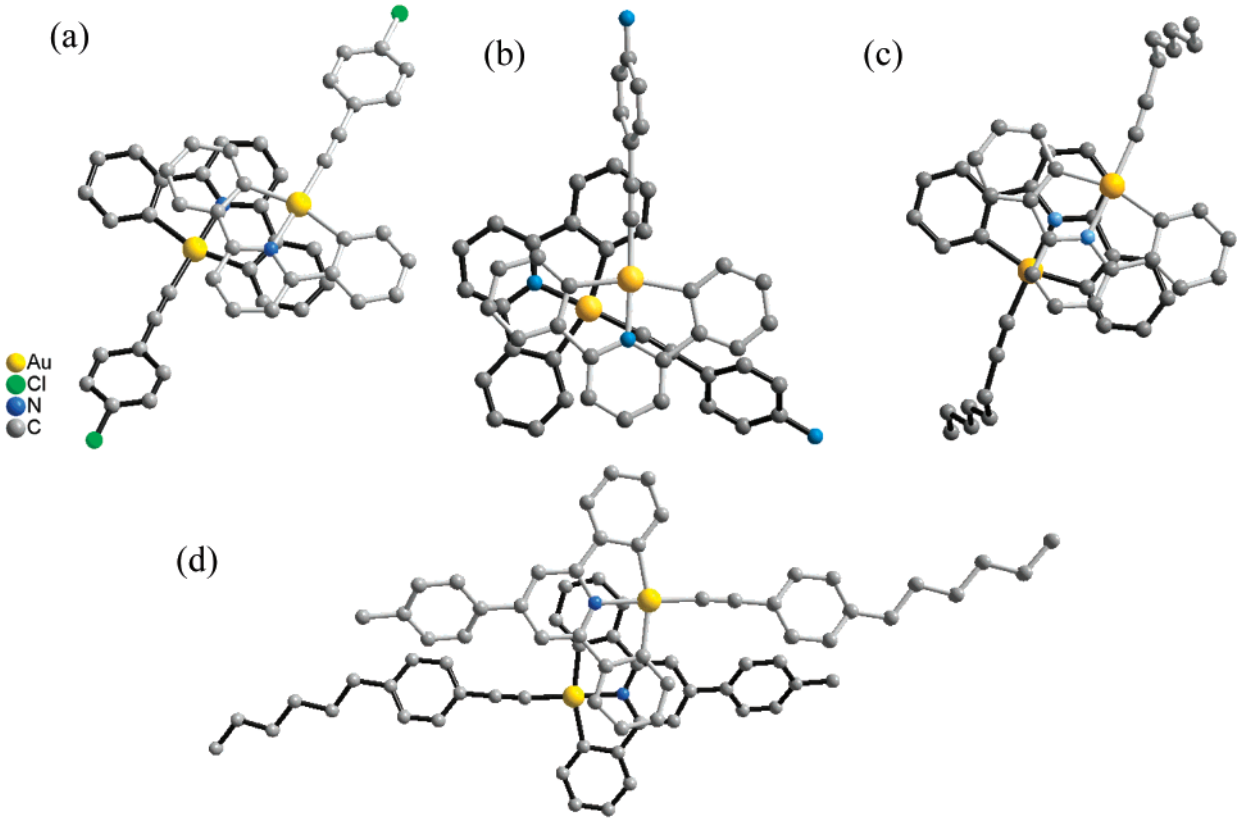

Figure 3. Crystal packing diagrams of **2** (a), **5** (b), **7** (c), and **9** (d) showing the dimeric configuration.

Table 4. Electrochemical Data for **1**−**9**[a]

complex	oxidation E_{pa}[b]/V vs SCE	reduction $E_{1/2}$[c] /V vs SCE
1	+1.57, +1.75	−1.57
2	+1.57, +2.13	−1.59
3	+1.96	−1.08, −1.52, −1.64
4	+1.15, +2.07	−1.58
5	+0.76, +1.87	−1.59
6	+1.34, +2.02	−1.58
7	+1.68, +2.17	−1.69
8	+1.59, +2.15	−1.64
9	+1.27, +2.13	−1.52

[a] In dichloromethane solution with 0.1 M $^{n}Bu_4NPF_6$ (TBAH) as supporting electrolyte at room temperature; scan rate 100 mV s^{-1}. [b] E_{pa} refers to the anodic peak potential for the irreversible oxidation waves. [c] $E_{1/2} = (E_{pa} + E_{pc})/2$; E_{pa} and E_{pc} are peak anodic and peak cathodic potentials, respectively.

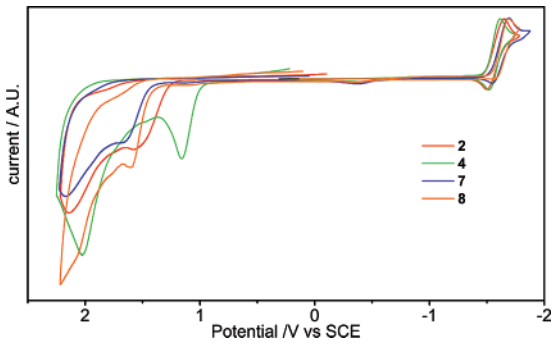

Figure 4. Cyclic voltammograms of **2**, **4**, **7**, and **8** in CH_2Cl_2 (0.1 mol dm^{-3} $^{n}Bu_4NPF_6$).

(R′)^CR ligand, probably mixed with the LLCT transitions given the nonreducing nature of the gold(III) metal center which eliminates the possibility of a metal-to-ligand charge transfer (MLCT) transition. Similar assignments have also been reported for other related gold(III) complexes.[6d]

In the case of complex **3**, a much more intense absorption band located at 327 nm was observed which is attributed to the IL $\pi-\pi^*$ transition of alkynyl ligand due to the presence of the nitro substituent. It is noteworthy that an additional shoulder was observed in the electronic absorption spectrum of **5** at about 415−435 nm. In view of the better electron-donating ability of the electron-rich amino substituent on the alkynyl ligand, a low-lying alkynyl-to-RC^N(R′)^CR ligand-to-ligand charge-transfer (LLCT) transition becomes feasible and appears as a shoulder at 415 nm. The low-energy absorptions in **5** are therefore assigned as an admixture of IL [$\pi \rightarrow \pi^*$ (C^N^C)]/LLCT [π-(C≡C$C_6H_4NH_2$) → π^*(C^N^C)] transitions. Complex **8**, which contains the same alkynyl ligand as **1**, shows a lower absorption energy relative to that of **1**. This is in accordance with the assignment of a metal-perturbed $\pi \rightarrow \pi^*$(RC^N(R′)^CR) intraligand (IL) transition since the electron-donating *tert*-butyl groups on the phenyl rings would narrow the HOMO−LUMO energy gap in view of the fact that the energy level of the HOMO π orbital is raised to a larger extent than that of the LUMO π^* orbital. Similarly, the observation of a lower-energy $\pi \rightarrow \pi^*$ IL transition in **9** relative to that of **6** is ascribed to the stabilization of the π^* orbital by the better delocalization over the C^NTol^C ligand upon introduction of the tolyl group on the pyridine ring, which results in a narrowing of the $\pi-\pi^*$ energy gap.

Luminescence Spectroscopy. The photoluminescence properties of this class of alkynylgold(III) complexes have been previously communicated.[7a] Upon excitation at λ > 360 nm,

Table 5. Photophysical Data for **1**−**9**

complex	absorption[a] λ_{max}/nm (ϵ_{max}/dm^3 mol^{-1} cm^{-1})	emission medium (T/K)	emission λ_{max}/nm (τ_o/μs)	Φ_{em}[b]
1	312 (19890), 322 (19980), 364 (5050), 381 (5870), 402 (4870)	CH_2Cl_2 (298)[c]	476, 506, 541, 582 (<0.05)	1.0×10^{-3}
		solid (298)	588 (<0.05)	
		thin film (298)[d]	568 (<0.05)	
		solid (77)	496 (28.3, 310.4)[f]	
		glass (77)[c,e]	470, 503, 537, 585 (194)	
2	312 (19400), 322 (19640), 365 (4640), 382 (5170), 402 (4305)	CH_2Cl_2 (298)[c]	476, 506, 539, 584 (<0.05)	2.0×10^{-4}
		solid (298)	550 (<0.05)	
		solid (77)	500 (25.3, 256.6)[f]	
		glass (77)[c,e]	470, 504, 534, 590 (151)	
3	312 (26800), 327 (36100), 363 (18545), 382 (10260), 402 (5720)	CH_2Cl_2 (298)[c]	478, 508, 540, 600 (0.3)	1.9×10^{-3}
		solid (298)[c]	565 (<0.05)	
		solid (77)	515, 550, 600 (0.6)	
		glass (77)[c,e]	472, 508, 539, 590 (189, 923)[f]	
4	312 (13820), 322 (13455), 362 (6400), 380 (6245), 400 (4190)	CH_2Cl_2 (298)[c]	474, 505, 539, 584 (<0.05)	5.0×10^{-4}
		solid (298)	555 (<0.05)	
		solid (77)	485 (28.4, 268.2)[f]	
		glass (77)[c,e]	470, 503, 536, 585 (137)	
5	310 (19195), 322 sh (15680), 365 (8855), 381 (10100), 399 (8300), 415 sh (3410)	CH_2Cl_2 (298)	611 (0.3)	2.0×10^{-3}
		solid (298)	585 (0.2)	
		solid (77)	548 (0.3, 1.7)[f]	
		glass (77)[c,e]	470, 503, 535, 587 (107)	
6	313 (18010), 323 (18240), 363 (5130), 381 (5250), 401 (3940)	CH_2Cl_2 (298)[c]	474, 508, 546, 585 (<0.05)	2.0×10^{-3}
		solid (298)[c]	562 (<0.05)	
		solid (77)	513, 552, 600 (28.7, 227.6)[f]	
		glass (77)[c,e]	470, 504, 534, 590 (142)	
7	311 (14860), 320 (14040), 364 (3800), 380 (4840), 400 (4230)	CH_2Cl_2 (298)[c]	471, 508, 535, 553 (<0.05)	1.9×10^{-3}
		solid (298)[c]	561 (<0.05)	
		solid (77)	513, 533, 585 (32.4, 274.1)[f]	
		glass (77)[c,e]	469, 503, 535, 585 (221)	
8	313 (26190), 323 (24460), 374 (6130), 392 (8035), 412 (7465)	CH_2Cl_2 (298)[c]	484, 514, 548, 593 (0.1)	6.0×10^{-3}
		solid (298)	550 (<0.05)	
		solid (77)	503 (18.2, 171.9)[f]	
		glass (77)[c,e]	478, 512, 548, 600 (200)	
9	290 (42660), 304 (40780), 330 (25220), 364 (6100), 386 (5120), 406 (3540)	CH_2Cl_2 (298)[c]	475, 505, 547, 592 (<0.05)	2.7×10^{-3}
		solid (298)[c]	563 (<0.05)	
		solid (77)	552 (25.6, 177.9)[f]	
		glass (77)[c,e]	470, 505, 540, 585 (83)	

[a] In dichloromethane at 298 K. [b] The luminescence quantum yield, measured at room temperature using $[Ru(bpy)_3]^{2+}$ as a standard. [c] Vibronic-structured emission band. [d] Prepared by vacuum deposition. [e] In CH_2Cl_2/EtOH/MeOH (1:40:10 v/v). [f] Double exponential decay.

solid samples and dichloromethane solutions of the alkynylgold(III) complexes exhibit intense luminescence at 470−611 nm at both room temperature and 77 K. The photophysical data of **1**−**9** are tabulated in Table 5. Compared to the chloro analogue, [Au(C^N^C)Cl], which are reported to emit only in low-temperature glasses, the enrichment of the luminescence behaviors of **1**−**9** demonstrates the concept that incorporation of strong σ-donating alkynyl ligands into gold(III) could enlarge the d−d ligand field splitting, giving rise to an enhancement of their luminescence properties. Figure 6 depicts the emission spectra of **1**, **5**, **8**, and **9** in dichloromethane solution at room temperature. The long-lived emission with lifetimes in the submicrosecond to microsecond range, together with the observed large Stokes shift, suggests that the emission is of triplet parentage. In dichloromethane solution at room temperature, almost identical spectra were observed in **1**−**4**, **6**, and **7** which contain the same C^N^C ligand, in which a vibronic-structured emission band with a band maximum at around 480 nm was observed. These findings suggest that the emission energies of the compounds are rather insensitive to the nature of the alkynyl ligands. The vibrational progressional spacings of about 1300 cm^{-1} are characteristic of the C═C and C═N stretching frequencies of the tridentate ligand, indicative of the involvement of the tridentate RC^N(R′)^CR ligand in the excited-state origin. The luminescence is assigned as originating from a metal-perturbed $^3[\pi \rightarrow \pi^*$(RC^N(R′)^CR)] IL state. Similar assignment has also been made in other related mononuclear [Au(C^N^C)X] complexes.[6d] Parallel to the electronic absorption study, the observation of the emission band of **8** at lower energy than that of **1** is ascribed to the narrower $\pi-\pi^*$ energy separation of the RC^N(R′)^CR ligand due to the attachment of the electron-donating *tert*-butyl groups on the phenyl rings (Figure 6). Although the introduction of the tolyl group on the pyridyl ring of the C^NTol^C ligand in **9** is anticipated to lower the π^* orbital energy of the C^NTol^C ligand as discussed in the electronic absorption study, only a very small to negligible shift of this vibronic-structured emission band was observed in **9**. Unlike the other members of this series of alkynylgold(III) complexes, which in general show a vibronic-structured emission band in dichloromethane, **5** with an amino-phenyl alkynyl group shows a lower-energy structureless emission band centered at ca. 610 nm (Figure 6). This structureless emission band

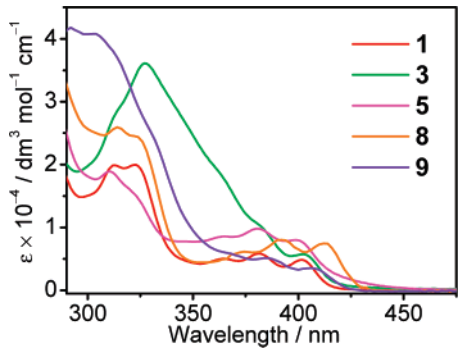

Figure 5. Electronic absorption spectra of **1**, **3**, **5**, **8**, and **9** in CH_2Cl_2 at room temperature.

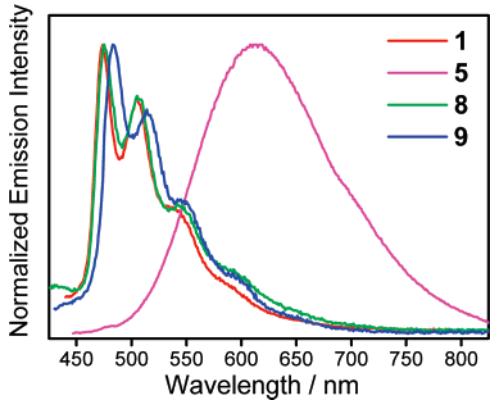

Figure 6. Emission spectra of **1**, **5**, **8**, and **9** in degassed CH_2Cl_2 at room temperature.

was found to be concentration-independent in the range 5×10^{-6} to 1×10^{-3} mol dm^{-3}, suggesting that excimeric emission arising from the $\pi-\pi$ stacking of the C^N^C motifs in solution is unlikely. On the basis of the energetically higher-lying π-($C{\equiv}CC_6H_4{-}NH_2$) orbital resulting from the strong electron-donating amino substituent, the lower-energy emission band in **5** is tentatively assigned as derived from an excited state of ^{3}LLCT [$\pi(C{\equiv}CC_6H_4NH_2) \rightarrow \pi^*$(C^N^C)] origin. Such an assignment is further corroborated by the computational studies (vide infra) as well as the assignment of the first oxidation wave in the electrochemical study as an alkynyl ligand-centered oxidation. On the contrary, **1**−**9** exhibit a broad low-energy emission band at 550−585 nm in the solid state at ambient temperature. The structureless band shape and the red shift of the solid-state emission band relative to that in dichloromethane solution are attributed to the $\pi-\pi$ excimeric ^{3}IL emission due to the $\pi-\pi$ stacking interaction of the C^N^C ligand in the solid state, as revealed by the ordered packing of the molecules in the X-ray crystal packings of the complexes.

For emission studies in low-temperature glasses, all the complexes show similar vibronic-structured emission bands with an emission energy similar to that observed in dichloromethane solution. It is interesting to note that the emission spectrum of **5** in 77 K glass also exhibits a similar vibronic-structured emission band, in contrast to that recorded in dichloromethane solution, in which a structureless emission band was observed. The change of emission origin in **5** from the ^{3}LLCT [$\pi(C{\equiv}CC_6H_4NH_2) \rightarrow \pi^*$(C^N^C)] excited state to the metal-perturbed ^{3}IL [$\pi \rightarrow \pi^*$ (C^N^C)] excited state by a lowering of the medium temperature indicates that these two excited states are close-lying in energy.

Computational Studies. In order to gain further insights into the structural, electrochemical, and photophysical properties as well as the electronic structures of the ground and excited states of this series of luminescent alkynylgold(III) complexes, density functional theory (DFT) calculations at the B3LYP level of theory were performed to study complexes **1**−**5** and **7**−**9** (for details, see the Experimental Section). For the sake of reducing the computational cost, model complexes, [Au(C^N^C)($C{\equiv}C{-}CH_3$)] **7′** and [Au(C^NTol^C)($C{\equiv}CC_6H_4{-}CH_3$-*p*)] **9′**, respectively, were used instead of complexes **7** and **9**, in which the hexyl group on the phenyl alkynyl ligand and the alkynyl ligand were replaced by a methyl group.

Geometry optimizations were performed for the two extreme forms of complexes **1**−**5**, **8**, and **9′**, i.e., perpendicular (the aryl rings lie perpendicular to the RC^N(R′)^CR plane) and coplanar forms (the aryl rings lie in the plane of the RC^N(R′)^CR ring), which were labeled as **1a**−**5a**, **8a**, and **9′a** and **1b**−**5b**, **8b**, and **9′b**, respectively. The energy difference between the two forms in each complex is quite small, in which the perpendicular forms of complexes **1**−**3**, **8**, and **9′** are relatively more stable than the corresponding coplanar forms by 0.1−0.6 kcal mol^{-1}, while the coplanar forms are more stable than the perpendicular forms by 0.1 and 0.3 kcal mol^{-1} in complexes **4** and **5**, respectively. This may account for the observation of both conformations in their crystal structures. The optimized geometries of **1a**−**5a**, **8a**, and **9′a** with selected structural parameters as well as the experimental structural parameters of **1**−**5**, **8**, and **9** are shown in Figure 7 (see Table S1 for the selected structural parameters of the planar forms). In general, the calculated bond lengths and angles of **1**−**5**, **7′**, **8**, and **9′** are in good agreement with that observed in the X-ray crystal structures (see Figure 7 and Table S1), implying that the level of theory and basis sets that we applied are reliable.

As the effect of the substituents R, R′, and R″ on the change of the molecular orbital energies in both structural forms of **1**−**5**, **8**, and **9′** is similar, for our convenience, only molecular orbitals in the perpendicular forms with the symbol "**a**" will be considered in the discussion of molecular orbitals. Figure 8 shows the spatial plots of selected TDDFT/CPCM frontier orbitals in **1a**. These orbitals were found to be involved in the electronic transitions (vide infra). As depicted, the frontier filled orbitals were mainly contributed by the π systems of the phenyl alkynyl and the C^N^C ligands. The HOMO ($\pi_{C{\equiv}CC_6H_5}$) and HOMO−3 ($\pi_{C{\equiv}CC_6H_5\ orth}$) are the two orthogonal sets of π orbitals on the alkynyl. The remaining filled orbitals are mainly π orbitals of the C^N^C ligand, which are HOMO−1 ($4\pi_{C^N^C}$), HOMO−2 ($3\pi_{C^N^C}$), HOMO−6 ($2\pi_{C^N^C}$), and HOMO−7 ($1\pi_{C^N^C}$). The unoccupied molecular orbitals LUMO and LUMO+1 are essentially π^* orbitals localized on the C^N^C ligand, where they are denoted $1\pi^*_{C^N^C}$ and $2\pi^*_{C^N^C}$, with a larger contribution on the pyridine ring. The LUMO+2 consists of a σ-antibonding interaction between the metal center and the coordinated ligands (σ^*_{AuL}).

The energies of the frontier orbitals in **1a** as well as the corresponding orbitals in **2a**−**5a**, **7′**, **8a**, and **9′a** and the percentage compositions of these frontier orbitals are listed in Table 6 and Table S3, respectively. The corresponding information for the coplanar forms are listed in Tables S2 and S3, respectively. The energy of the HOMO ($\pi_{C{\equiv}CR''}$) in all the complexes with the aryl alkynyl ligand was found to show a

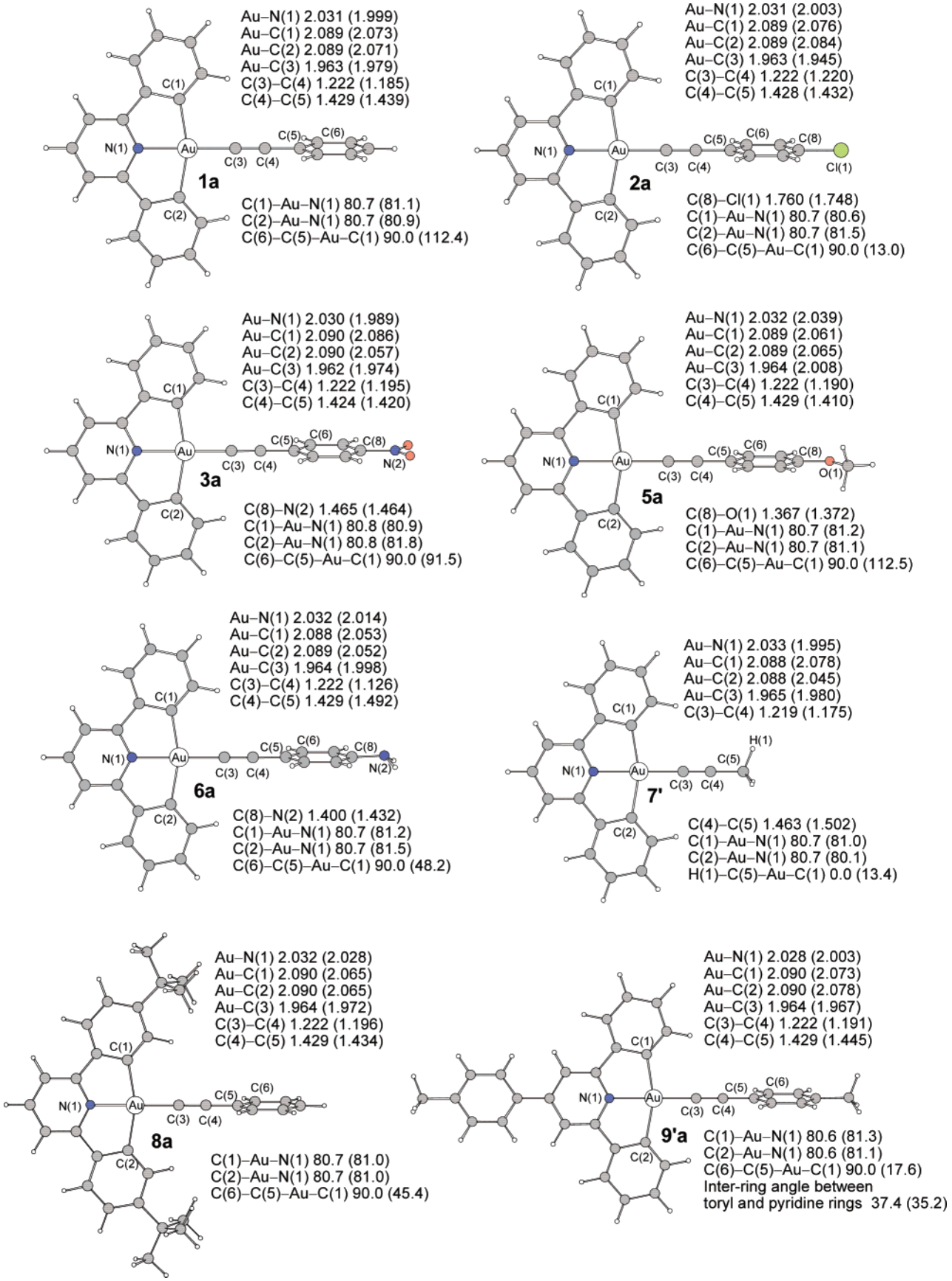

Figure 7. Selected structural parameters of the B3LYP optimized geometries for **1a**−**5a**, **7′**, **8a**, and **9′a** with the experimental structural parameter shown in parentheses.

strong dependence on the nature of the substituents at the *para* position of the phenyl alkynyl group. Especially for the −OMe and $-NH_2$ groups in **4a** and **5a**, the HOMO energy was found to increase by 0.33 and 0.69 eV in **4a** and **5a**, respectively,

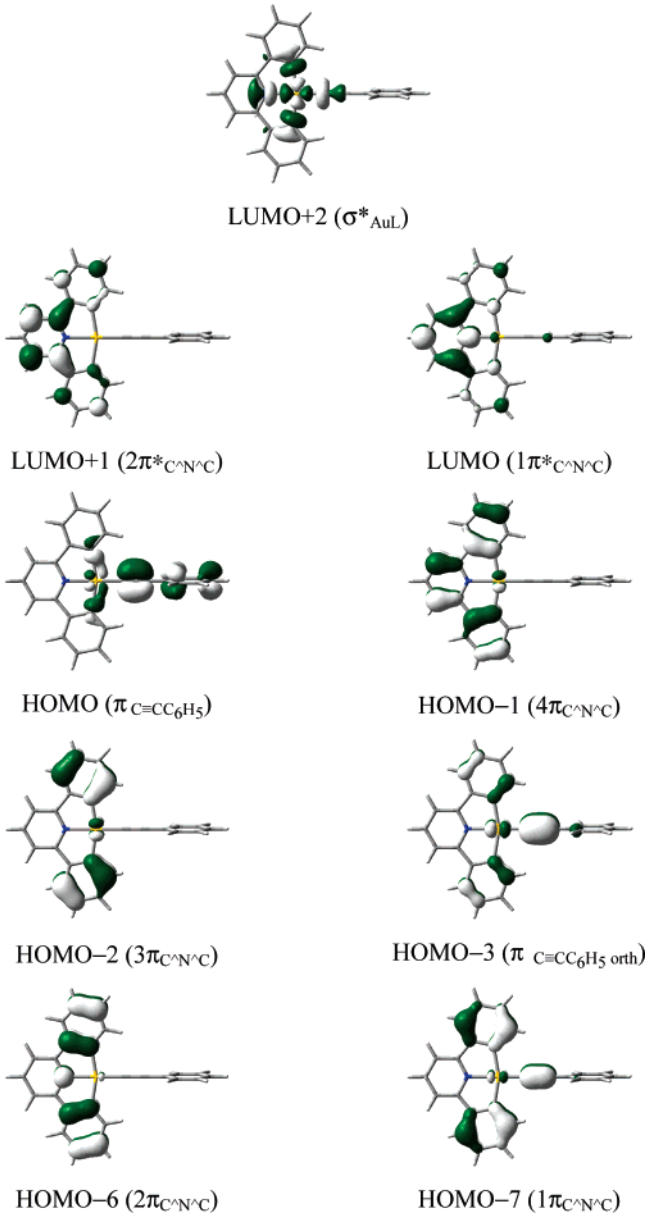

Figure 8. Spatial plots (isovalue = 0.04) of the selected TDDFT/CPCM frontier molecular orbitals of **1a**.

when compared to that in **1a**. These can be explained by the strong electron-donating abilities of the methoxy and amino groups, which significantly raise the HOMO energy. On the other hand, the HOMO energy was found to decrease significantly by 0.41 eV in **3a**, when compared to that in **1a**, because of the strong electron-withdrawing ability of the NO_2 group. These results are in agreement with the CV study, in which **3** is the most difficult to be oxidized, while **5** is the easiest to be oxidized.

Unlike the LUMO of **1a** and the other complexes ($1\pi^*_{RC^N(R')^CR}$), the LUMO of **3a** consists mainly of the π^* orbital localized on the $C\equiv CC_6H_4-NO_2$ ligand (denoted as $\pi^*_{C\equiv CC_6H_4NO_2}$), with an energy of 0.37 eV lower than that of the $1\pi^*_{C^N^C}$ orbital (LUMO+1). The occurrence of the $\pi^*_{C\equiv CC_6H_4NO_2}$ orbital at lower energy than the $1\pi^*_{C^N^C}$ orbital is consistent with the additional reduction wave observed at a less negative potential (−1.08 V) in **3** from the electrochemical study. The energy of the LUMO of **8a** is slightly increased by

Table 6. TDDFT/CPCM Orbital Energies (eV) in **1a**−**5a**, **7′**, **8a**, and **9′a**

	1a	2a	3a	4a	5a	7′	8a	9′a
σ^*_{AuL}	−0.68	−0.72	−0.80	−0.66	−0.62	−0.61	−0.64	−0.65
$2\pi^*_{RC^N(R')^CR}$	−1.56	−1.58	−1.61	−1.55	−1.54	−1.54	−1.52	−1.56
$1\pi^*_{RC^N(R')^CR}$	−2.11	−2.13	−2.17	−2.10	−2.08	−2.07	−2.05	−2.19
$\pi_{C\equiv CR''}$	−5.72	−5.80	−6.14	−5.40	−5.04	−6.09	−5.68	−5.61
$4\pi_{RC^N(R')^CR}$	−6.12	−6.14	−6.18	−6.12	−6.10	−6.10	−5.99	−6.12
$3\pi_{RC^N(R')^CR}$	−6.67	−6.69	−6.73	−6.66	−6.65	−6.65	−6.58	−6.65
$\pi_{C\equiv CR''\ orth}$	−6.71	−6.79	−6.92	−6.69	−6.62	−6.50	−6.60	−6.71
$2\pi_{RC^N(R')^CR}$	−6.84	−6.87	−6.88	−6.83	−6.82	−6.82	−6.68	−6.84
$1\pi_{RC^N(R')^CR}$	−7.10	−7.14	−7.25	−7.08	−7.05	−7.03	−7.01	−7.10

0.06 eV, compared to that of **1a**, which is ascribed to the presence of electron-donating *tert*-butyl substituents on the phenyl rings in the $^tBuC^N^C^tBu$ ligand. On the other hand, on going from **1a** to **9′a**, the energy of the LUMO is decreased by 0.08 eV, due to the increase in the extent of π-conjugation upon attachment of the tolyl group to the pyridine ring in the C^NTol^C ligand. The energy of the HOMO in **7′** is decreased significantly, compared to that in **1a**, as a result of the presence of the antibonding interaction between the π orbitals on the C≡C triple bond and the attached phenyl group in **1a** that would increase the HOMO energy, which is absent in **7′**. On the other hand, the LUMO energy is increased from **1a** to **7′**. Presumably, the more electron-rich aliphatic alkynyl ligand would render the metal center more electron-rich, raising the metal dπ orbital energy, leading to a better energy match between the metal dπ orbital and the π^* orbital of the C^N^C ligand that gave rise to a higher-lying LUMO. The observed trends are consistent with the electrochemical data.

A nonequilibrium TDDFT/CPCM calculation using CH_2Cl_2 as the solvent was employed to investigate the nature of the singlet excited states in the aryl alkynyl Au(III) complexes **1**−**5**, **8**, and **9′** with both the perpendicular and coplanar forms, and the aliphatic alkynyl Au(III) complex **7′** (see Experimental Section). The selected singlet−singlet excitations of complexes **1a** and **1b** in the range detected in the absorption spectra are shown in Table 7. The nature of the orbitals involved in the excitation[13] is also shown, where the same convention is used as that in the previous section (see Figure 8). The spectral assignment is based on the correlation of the experimental band maxima with the calculated excited-state energies of the transitions with the oscillator strength greater than 0.005.

From the calculation results, there are two types of transitions at the low-energy absorption region which resemble those observed in the experimental UV−visible absorption spectra. The low-energy allowed transitions located at ca. 380 and 370 nm can be assigned as the metal-perturbed intraligand IL transitions [$4\pi_{C^N^C} \rightarrow 1\pi^*_{C^N^C}$] ($S_2$ state in **1a** and S_1 state in **1b**) and the metal-perturbed ligand-to-ligand charge-transfer LLCT [$\pi_{C\equiv CC_6H_5} \rightarrow 1\pi^*_{C^N^C}$] transitions [this transition is forbidden in **1a** (S_1 state),[14] but it is allowed in **1b** (S_2 state)], respectively. Several transitions are computed in the high-energy absorption region of **1**. They mainly consist of the contributions from the IL $\pi-\pi^*$ transitions of the C^N^C ligand and the

(13) The character of each excited state is assigned according to the compositions of the occupied and virtual MOs of the dominant configuration (s) for that excited state. Different from the one-electron excitation model, the TDDFT formalism regards excited states as linear combinations of singly excited determinants. Accordingly, each transition includes a series of excitations, where some of them outweigh the others and predominate the character of the transitions.

Table 7. Selected Low-Lying Singlet (S_n) Excited States Computed by TDDFT/CPCM, with the Orbitals Involved in the Excitations, Transition Coefficients, Vertical Excitation Energies (eV and nm), and Oscillator Strengths (*f*) in **1a** and **1b**

1a						**1b**					
			vertical excitation energy						vertical excitation energy		
S_n	excitation[a]	transition coefficient	eV	nm	f[b]	state	excitation[a]	transition coefficient	eV	nm	oscillator strength[b]
S_2	$4\pi_{C\wedge N\wedge C} \rightarrow 1\pi^*_{C\wedge N\wedge C}$	0.68	3.27	380	0.06	S_1	$4\pi_{C\wedge N\wedge C} \rightarrow 1\pi^*_{C\wedge N\wedge C}$	0.68	3.25	381	0.05
S_5	$3\pi_{C\wedge N\wedge C} \rightarrow 1\pi^*_{C\wedge N\wedge C}$	0.67	3.95	314	0.17	S_3	$\pi_{C\equiv CC_6H_5} \rightarrow 1\pi^*_{C\wedge N\wedge C}$	0.70	3.35	370	0.22
S_6	$\pi_{C\equiv CC_6H_5\ orth} \rightarrow 1\pi^*_{C\wedge N\wedge C}$	0.68	4.03	308	0.16	S_4	$3\pi_{C\wedge N\wedge C} \rightarrow 1\pi^*_{C\wedge N\wedge C}$	0.63	3.93	315	0.13
S_7	$2\pi_{C\wedge N\wedge C} \rightarrow 1\pi^*_{C\wedge N\wedge C}$	0.68	4.13	300	0.01	S_5	$\pi_{C\equiv CC_6H_5} \rightarrow 2\pi^*_{C\wedge N\wedge C}$	0.66	3.95	314	0.05
S_8	$4\pi_{C\wedge N\wedge C} \rightarrow 2\pi^*_{C\wedge N\wedge C}$	0.57	4.14	299	0.10	S_7	$2\pi_{C\wedge N\wedge C} \rightarrow 1\pi^*_{C\wedge N\wedge C}$	0.59	4.10	303	0.10
S_9	$\pi_{C\equiv CC_6H_5} \rightarrow \sigma^*_{AuL}$	0.67	4.23	293	0.06	S_8	$4\pi_{C\wedge N\wedge C} \rightarrow 2\pi^*_{C\wedge N\wedge C}$	0.48	4.12	301	0.07
S_{11}	$1\pi_{C\wedge N\wedge C} \rightarrow 1\pi^*_{C\wedge N\wedge C}$	0.59	4.48	277	0.22	S_{11}	$1\pi_{C\wedge N\wedge C} \rightarrow 1\pi^*_{C\wedge N\wedge C}$	0.55	4.47	283	0.18

[a] The excitations with the transition coefficients less than 0.4 were not shown. [b] Only the singlet excited states with $f > 0.005$ were listed.

LLCT transitions from π orbitals on the C≡C triple bond of the alkynyl unit to the π^* orbitals on the C^N^C ligand. In general, the calculated singlet−singlet transitions in **2**−**5**, **7′**, **8**, and **9′** are similar to that in **1** and are shown in Tables S4−S10.

Basically, the calculated singlet−singlet transitions in **1**−**5**, **7′**, **8**, and **9** are in reasonable agreement with the experimental λ_{max} in the two major electronic absorption bands observed in the experimental spectra. For **5b**, a significant red shift of the LLCT [$\pi_{C\equiv CC_6H_4NH_2} \rightarrow 1\pi_{C\wedge N\wedge C}$] transition is found at 459 nm relative to **1b** and it becomes 0.58 eV lower in energy than its IL [$4\pi_{C\wedge N\wedge C} \rightarrow 1\pi^*_{C\wedge N\wedge C}$] transition, which might account for the additional shoulder that appeared in the electronic absorption spectrum of **5** at about 415−435 nm. The low-energy IL [$4\pi_{RC\wedge N(R')\wedge CR} \rightarrow 1\pi^*_{RC\wedge N(R')\wedge CR}$] transitions are found to be red-shifted in **8** (385 nm in **8a** and 387 nm in **8b**) and **9′** (387 nm in **9′a** and 388 nm in **9′b**) relative to **1** (380 nm in **1a** and 381 nm in **1b**), which is in agreement with the observed trend of the experimental λ_{max} (381 nm for **1**, 392 nm for **8**, and 386 nm for **9**) in the lower-energy absorption band. This can be explained by the electron-donating ability of the ^{t}Bu groups attached to the two phenyl rings in the ^{t}BuC^N^C^{t}Bu ligand and the extended π-conjugation upon introduction of the tolyl group attached to the pyridine ring in the C^NTol^C ligand which destabilizes the $4\pi^*_{^tBuC\wedge N\wedge C^tBu}$ orbital more relative to the $1\pi^*_{^tBuC\wedge N\wedge C^tBu}$ orbital and stabilizes the $1\pi^*_{C\wedge N(Tol)\wedge C}$ orbital, respectively, and thus narrows the gap for the IL [$4\pi_{RC\wedge N(R')\wedge CR} \rightarrow 1\pi^*_{RC\wedge N(R')\wedge CR}$] transition.

In order to study the nature of the emitting triplet states and the structural changes from the corresponding ground states of the Au(III) complexes, an unrestricted Kohn−Sham approach (UB3LYP) was used to optimize the low-lying triplet states in **1**−**5**, **7′**, **8** and **9′**. For some of the complexes, optimization of the triplet states starting from the ground-state perpendicular structure gave a highly distorted structure, in which the C^N^C ligand is unrealistically distorted. As a consequence, only the triplet states, which were optimized starting from the ground-state coplanar structures, would be considered here. Figure 9 shows the optimized structure of the triplet excited state of **1** and selected changes in the structural parameters relative to that of the ground state. The major geometrical changes occur mainly

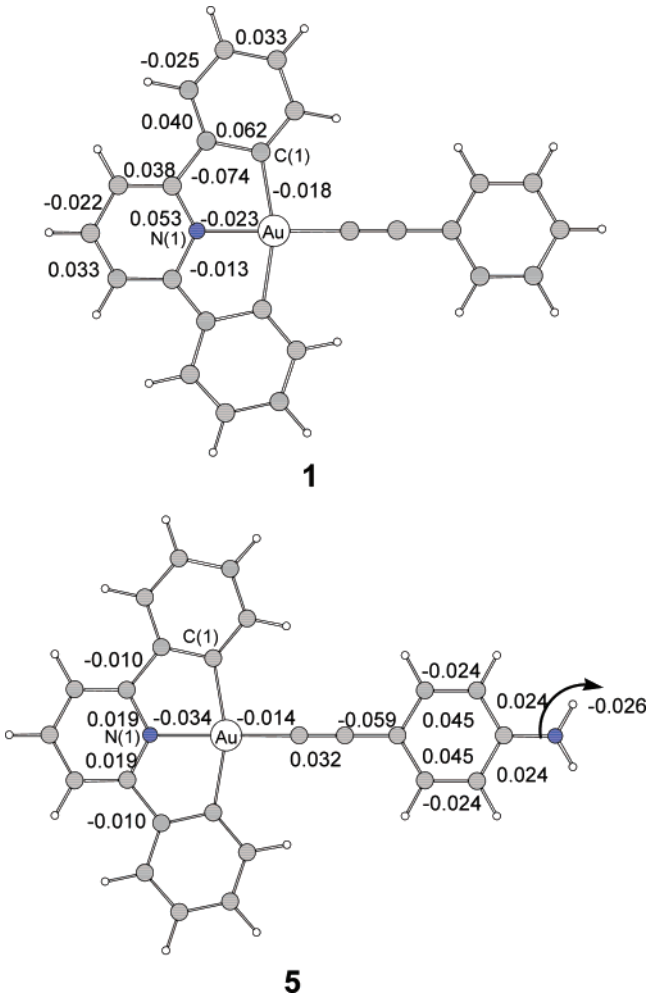

Figure 9. Optimized structures of the triplet states of in **1** and **5** starting from the ground-state coplanar structures with the change in bond distances (in Å), relative to their corresponding ground states. Only differences in bond distances larger than 0.01 Å were shown.

in the C(1) phenyl ring and the pyridine ring in the C^N^C ligand. Inspection of the two singly occupied molecular orbitals (SOMOs) of the optimized triplet excited state of **1** reveals that the lower- and higher-energy SOMOs are contributed mainly from the π and π^* orbitals of the C^N^C ligand, respectively (see Figure S1). This provides a clear indication that the triplet excited state of **1** contains the IL [$\pi \rightarrow \pi^*$ (C^N^C)] character. However, optimization of the triplet state of complex **5** gave a different type of distortion, in which the major change in the triplet excited state of **5** occurs mainly in the metal-pyridine

(14) The low intensity of the $S_0 \rightarrow S_1$ transition is presumably associated with a symmetry restriction. Consider the molecule having a C_{2v} symmetry, the irreducible representations of the HOMO ($\pi_{C\equiv CC_6H_5}$) and LUMO ($1\pi^*_{C\wedge N\wedge C}$) are b_2 and b_1, respectively. The HOMO−LUMO transition ($b_2 \rightarrow b_1$) generates the $^1A_2$ excited state. As no electronic dipole moment component belongs to A_2 symmetry, this transition is forbidden.

Table 8. Calculated and Experimental Emission Maxima for Selected Complexes

complex	calculated emission maximum (λ_{calcd})/nm[a]	experimental emission maximum (λ_{max}) in CH_2Cl_2 at 298 K/nm
1	466	476
2	466	476
3	471	476
4	466	474
5	520	611
7′	465	471
8	472	484
9′	466	478

[a] The energy difference with solvent correction (CH_2Cl_2) between the optimized ground and triplet excited states (^{3}IL [$\pi\rightarrow\pi^*$ (RC^N(R′)^CR)] state for **1**−**4**, **7′**, **8**, and **9′** and ^{3}IL [$\pi\rightarrow\pi^*$ ($C\equiv CC_6H_4NH_2$)]/^{3}LLCT [π ($C\equiv CC_6H_4NH_2$) $\rightarrow \pi^*$ (C^N^C)] state for **5**) of the coplanar forms.

and metal-aryl ethynyl units (see Figure 9), suggesting a difference in the nature of the excited states. In the triplet excited state of **5**, the lower-energy SOMO is mainly a π orbital on the $C\equiv CC_6H_4-NH_2$ unit, while the higher-energy SOMO is the π^* orbital localized on the C^N^C and $C\equiv CC_6H_4-NH_2$ ligand (see Figure S1). This indicates that the excited state contains admixtures of ^{3}IL [$\pi \rightarrow \pi^*$ ($C\equiv CC_6H_4NH_2$)] character and ^{3}LLCT [$\pi(C\equiv CC_6H_4NH_2) \rightarrow \pi^*$(C^N^C)] character.

Table 8 shows the calculated emission maxima of **1**−**5**, **7′**, **8**, and **9′**, estimated from the difference in the solvent-corrected energy of the ground and triplet-excited states (see Experimental Section). The calculated emission maxima of ^{3}IL [$\pi \rightarrow \pi^*$ (RC^N(R′)^CR)], corresponding to 465−471 nm (2.63−2.67 eV) for **1**−**4**, **7′**, and **9′** and 473 nm (2.62 eV) for **8**, correlated well with the experimental emission energies for the Au complexes with 471−478 nm for **1**−**4**, **7**, and **9** and 484 nm for **8**. A slight red shift of the triplet state energy was calculated in **8**, relative to **1**, which matches the trend observed in the experiments. The triplet state in **5** was calculated to be at 520 nm. Although the calculated emission energy was not in good agreement with that determined experimentally (620 nm), the switch in the nature of the excited state and the significant red shift in the calculated emissive state energy successfully mimic the trend observed in the experiments.

Conclusion

A new class of luminescent cyclometalated alkynylgold(III) complexes has been synthesized and characterized. The X-ray crystal structures of most of the complexes have been determined, and their crystal packings showed the presence of $\pi-\pi$ stacking interactions between adjacent RC^N(R′)^CR moieties. Electrochemical studies reveal an RC^N(R′)^CR ligand-centered reduction, with the exception of **3**, and an alkynyl ligand-centered oxidation. Their electronic absorption and luminescence behaviors have also been investigated. In dichloromethane solution at room temperature, the low-energy absorption bands are assigned as the $\pi-\pi^*$ intraligand (IL) transition of the cyclometalated RC^N(R′)^CR ligand with some mixing of a [$\pi(C\equiv CR'') \rightarrow \pi^*$(RC^N(R′)^CR)] ligand-to-ligand charge transfer (LLCT) character. The low-energy emission bands in dichloromethane solution at room temperature are ascribed to origins mainly derived from the $\pi-\pi^*$ IL transition of the cyclometalated RC^N(R′)^CR ligand. Complex **5**, which contains an electron-rich amino substituent on the alkynyl ligand, shows a low-energy [$\pi(C\equiv CC_6H_4NH_2) \rightarrow \pi^*$(C^N^C)] LLCT absorption. In contrast to the emission spectra in dichloromethane solution, a structureless and red-shifted emission band was observed in the solid state at room temperature, attributed to the $\pi-\pi$ excimeric ^{3}IL emission due to the $\pi-\pi$ interaction of the C^N^C ligand, as revealed by the observation of $\pi-\pi$ stacking in the crystal packings of the complexes in the solid state. The electronic structures of the ground and excited states for the luminescent alkynylgold(III) complexes **1**−**5** and **7**−**9** were studied by DFT calculations. The HOMO for all the complexes correspond to the π orbital on the alkyl/aryl alkynyl ligand, while the LUMO consists mainly of the π^* orbital on the RC^N(R′)^CR ligand with the exception of complex **3**, in which the LUMO is the π^* orbital localized on the $C\equiv CC_6H_4-NO_2$ ligand. These results are in agreement with the electrochemical study. The TDDFT/CPCM calculations indicate that the lowest energy absorption bands are attributed mainly to the metal-perturbed IL $\pi-\pi^*$ transition of the cyclometalated RC^N(R′)^CR ligand and metal-perturbed LLCT transition from the π orbital on the alkyl/aryl alkynyl ligands to the π^* orbital on the C^N^C ligand. The calculated emissive triplet states of all the complexes with the exception of complex **5** are derived predominantly from an IL [$\pi \rightarrow \pi^*$(RC^N(R′)^CR)] origin.

Experimental Section

Materials and Reagents. 1-Octyne, phenylacetylene, (4-aminophenyl)acetylene, (4-methoxyphenyl)acetylene, (4-hexylphenyl)acetylene, (4-nitrophenyl)acetylene, and (4-chlorophenyl)acetylene were purchased from Maybridge Chemical Co. Ltd. Potassium tetrachloroaurate(III) was purchased from Strem. Hg(C^N^CH)Cl (HC^N^CH = 2,6-diphenylpyridine),[6d] Au(C^N^C)Cl,[6d] 2,6-diphenyl-4-*p*-tolylpyridine,[15] and 2,6-bis(4-*tert*-butylphenyl)pyridine[15] were prepared by modification of the literature procedures. All solvents were purified and distilled using standard procedures before use. All other reagents were of analytical grade and were used as received. Tetra-*n*-butylammonium hexafluorophosphate (Aldrich) was recrystallized twice from absolute ethanol before use.

Physical Measurements and Instrumentation. UV−visible spectra were obtained on a Hewlett-Packard 8452A diode array spectrophotometer, and IR spectra, as a KBr disk on a Bio-Rad FTS-7 Fourier transform infrared spectrophotometer (4000−400 cm^{-1}). ^{1}H NMR spectra were recorded on a Bruker DPX-300 (300 MHz) or Bruker DPX-400 (400 MHz) Fourier transform NMR spectrometer with chemical shifts recorded relative to tetramethylsilane (Me_4Si). Positive-ion FAB or EI mass spectra were recorded on a Finnigan MAT95 mass spectrometer. Elemental analyses for the metal complexes were performed on the Carlo Erba 1106 elemental analyzer at the Institute of Chemistry, Chinese Academy of Sciences, Beijing, China. Steady-state excitation and emission spectra were recorded on a Spex Fluorolog-2 model F 111 fluorescence spectrofluorometer equipped with a Hamamatsu R-928 photomultiplier tube. All solutions for photophysical studies were prepared under a high vacuum in a 10-cm^3 round-bottomed flask equipped with a sidearm 1-cm fluorescence cuvette and sealed from the atmosphere by a Rotaflo HP6/6 quick-release Teflon stopper. Solutions were rigorously degassed on a high-vacuum line in a two-compartment cell with no less than four successive freeze−pump−thaw cycles. Solid-state photophysical measurements were carried out with the solid sample loaded in a quartz tube inside a quartz-walled Dewar flask. Liquid nitrogen was placed into the Dewar flask for low temperature (77 K) photophysical measurements. Excited-state lifetimes of solution samples were measured using a conventional laser system. The excitation source used was the 355-nm output (third harmonic, 8 ns) of a Spectra-Physics Quanta-Ray Q-switched GCR-150 pulsed Nd:YAG laser (10 Hz). Luminescence quantum yields were

(15) Kröhnke, F. *Synthesis* **1976**, 1.

measured by the optical dilute method reported by Demas and Crosby.[16a] A degassed aqueous solution of $[Ru(bpy)_3]Cl_2$ ($\Phi = 0.042$, excitation wavelength at 436 nm) was used as the reference.[16b]

Cyclic voltammetric measurements were performed by using a CH Instruments, Inc. model CHI 600A electrochemical analyzer. The electrolytic cell used was a conventional two-compartment cell. Electrochemical measurements were performed in acetonitrile solutions with 0.1 M ^{n}Bu$_4$NPF$_6$ (TBAH) as supporting electrolyte at room temperature. The reference electrode was a $Ag/AgNO_3$ (0.1 M in acetonitrile) electrode, and the working electrode was a glassy carbon electrode (CH Instruments, Inc.) with a platinum wire as the counter electrode. The working electrode surface was first polished with a 1-μm alumina slurry (Linde), followed by a 0.3-μm alumina slurry, on a microcloth (Buehler Co.). Treatment of the electrode surfaces was as reported previously.[17a] The ferrocenium/ferrocene couple ($FeCp_2^{+/0}$) was used as the internal reference.[17b] All solutions for electrochemical studies were deaerated with prepurified argon gas just before measurements.

Crystal Structure Determination. Single crystals of **1**−**5** and **7**−**9** suitable for X-ray diffraction studies were grown by slow diffusion of diethyl ether vapor into a dichloromethane solution of the complexes or by layering of *n*-hexane onto a concentrated dichloromethane solution of the complexes. The X-ray diffraction data were collected on a MAR diffractometer with a 300 mm image plate detector using graphite monochromatized Mo Kα radiation ($\lambda = 0.710\ 73$ Å). The images were interpreted and intensities were integrated using DENZO program.[18] The structure was solved by direct methods employing the SIR-97 program[19] (for **1** and **5**) or SHELXS-97 program[20] (**2**−**4** and **7**−**9**). Full-matrix least-squares refinement on F^2 was used in the structure refinement. The positions of H atoms were calculated based on the riding mode with thermal parameters equal to 1.2 times those of the associated C atoms and participated in the calculation of final *R*-indices. In the final stage of least-squares refinement, all non-hydrogen atoms were refined anisotropically.

Synthesis. Synthesis of [Hg(^{t}BuC^N^C^{t}BuH)Cl] (H^{t}BuC^N^C^{t}BuH = 2,6-Bis(4-*tert*-butylphenyl)pyridine). This was synthesized by modification of a literature procedure.[6d] A mixture of 2,6-bis(4-*tert*-butylphenyl)pyridine (1.51 g, 4.40 mmol) and mercury(II) acetate (1.40 g, 4.40 mmol) in absolute ethanol (30 mL) was heated under reflux for 24 h, and a solution of lithium chloride (0.37 g, 8.80 mmol) in methanol (20 mL) was then added. The mixture was heated for 15 min and was then added to distilled water (60 mL). The white precipitate was filtered off and washed with water and ice-cold methanol. The white solid was purified by column chromatography using *n*-hexane−ethyl acetate as eluent. Yield: 0.60 g (23%). ^{1}H NMR (300 MHz, CD_3SOCD_3, 298 K, relative to Me_4Si)/ppm: δ 1.33 (s, 18 H, ^{t}Bu), 7.45 (dd, 8.2 and 2.0 Hz, 1 H, phenyl of ^{t}BuC^N^C^{t}Bu), 7.50 (d, 8.5 Hz, 2 H, phenyl of ^{t}BuC^N^C^{t}Bu), 7.77 (d, 2.0 Hz, 1 H, phenyl of ^{t}BuC^N^C-^{t}Bu), 7.85 (d, 7.6 Hz, 1 H, pyridyl of ^{t}BuC^N^C^{t}Bu), 7.90 (d, 8.2 Hz, 1 H, phenyl of ^{t}BuC^N^C^{t}Bu), 7.91 (d, 1 H, 7.6 Hz, pyridyl of ^{t}BuC^N^C^{t}Bu), 7.99 (t, 7.6 Hz, 1 H, pyridyl of ^{t}BuC^N^C^{t}Bu), 8.06 (d, 8.5 Hz, 2 H, phenyl of ^{t}BuC^N^C^{t}Bu). Positive EI-MS: *m*/*z* 580 $[M]^+$. Elemental analyses calcd for $C_{25}H_{28}NClHg\cdot{}^1/_5C_6H_{14}$ (found): C, 52.82 (52.73); H, 5.21 (5.08); N, 2.35 (2.36).

Synthesis of [Hg(C^NTol^CH)Cl] (HC^NTol^CH = 2,6-Diphenyl-4-*p*-tolylpyridine). The procedure was similar to that for [Hg(^{t}BuC^N^C^{t}BuH)Cl], except 2,6-diphenyl-4-*p*-tolylpyridine was used in place of 2,6-bis(4-*tert*-butylphenyl)pyridine (1.41 g, 4.40 mmol). Yield: 0.78 g (32%). ^{1}H NMR (400 MHz, $CDCl_3$, 298 K, relative to Me_4Si)/ppm: δ 2.46 (s, 3 H, CH_3), 7.35 (d, 8.0 Hz, 2 H, phenyl of toly), 7.47−7.57 (m, 6 H, phenyl and pyridyl of C^NTol^CH), 7.66 (d, 8.0 Hz, 2 H, phenyl of toly), 7.91 (s, 1 H, pyridyl of C^NTol^CH), 7.98−8.00 (m, 3 H, phenyl of C^NTol^CH), 8.05 (dd, 7.1 and 2.0 Hz, 1 H, phenyl of C^NTol^CH). Positive FAB-MS: *m*/*z* 558 $[M]^+$. Elemental analyses calcd for $C_{24}H_{18}NClHg\cdot{}^1/_{10}C_6H_{14}$ (found): C, 52.29 (52.31); H, 3.46 (3.60); N, 2.48 (2.21).

[Au(^{t}BuC^N^C^{t}Bu)Cl]. This was synthesized according to the modification of a reported procedure.[6d] A mixture of Hg(^{t}BuC^N^C-^{t}BuH)Cl (0.60 g, 1.04 mmol) and $K[AuCl_4]$ (0.39 g, 1.04 mmol) in acetonitrile (60 mL) was refluxed for 24 h to afford a deep yellow solid. The solid was filtered and air-dried. Yield: 0.28 (47%). ^{1}H NMR (400 MHz, CD_3SOCD_3, 298 K, relative to Me_4Si)/ppm: δ 1.31 (s, 18 H, ^{t}Bu), 7.34 (dd, 8.2 and 2.0 Hz, 2 H, phenyl of ^{t}BuC^N^C^{t}Bu), 7.77 (d, 2.0 Hz, 2 H, phenyl of ^{t}BuC^N^C^{t}Bu), 7.79 (d, 8.2 Hz, 2 H, phenyl of ^{t}BuC^N^C^{t}Bu), 7.88 (d, 8.0 Hz, 2 H, pyridyl of ^{t}BuC^N^C^{t}Bu), 8.13 (t, 8.0 Hz, 1 H, pyridyl of ^{t}BuC^N^C^{t}Bu). Positive EI-MS: *m*/*z* 575 $[M]^+$. Elemental analyses calcd for $C_{25}H_{27}NAu$ (found): C, 52.29 (52.03); H, 4.71 (4.81); N, 2.44 (2.38).

[Au(C^NTol^C)Cl]. A mixture of Hg(C^NTol^CH)Cl (0.55 g, 0.99 mmol) and $K[AuCl_4]$ (0.37 g, 0.99 mmol) in acetonitrile (60 mL) was refluxed for 24 h to afford a deep yellow solid. The solid was filtered and air-dried. Yield: 0.23 (42%). ^{1}H NMR (400 MHz, CD_3SOCD_3, 298 K, relative to Me_4Si)/ppm: δ 2.44 (s, 3 H, CH_3), 7.34 (dt, 7.4 and 1.3 Hz, 2 H, phenyl of C^NTol^C), 7.42−7.46 (m, 4 H, phenyl of C^NTol^C), 7.71 (d, 7.4 Hz, 2 H, phenyl of C^NTol^C), 8.12 (d, 8.0 Hz, 4 H, phenyl of toly), 8.30 (s, 2 H, pryidyl of C^NTol^C). Positive FAB-MS: *m*/*z* 554 $[M]^+$. Elemental analyses calcd for $C_{24}H_{17}NClAu$ (found): C, 52.19 (51.91); H, 3.08 (2.98); N, 2.54 (2.46).

Syntheses of Alkynylgold(III) Complexes. All reactions were carried out under anaerobic and anhydrous conditions using standard Schlenk techniques.

[Au(C^N^C)(C≡CC$_6$H$_5$)] (1) by *Method a*. A mixture of [Au(C^N^C)Cl] (0.20 g, 0.43 mmol) and phenylacetylene (0.07 g, 0.65 mmol) in the presence of a catalytic amount of copper(I) iodide (9 mg) in triethylamine (2 mL) and dichloromethane (35 mL) was stirred at room tempearture for 3 h. After evaporation to dryness, the solid residue was purified by column chromatography on silica gel using dichloromethane as eluent. Subsequent recrystallization from slow diffusion of diethyl ether vapor into the concentrated solution gave **1** as pale yellow crystals. Yield: 0.20 g (88%). ^{1}H NMR (300 MHz, CD_2Cl_2, 298 K, relative to Me_4Si)/ppm: δ 7.26−7.44 (m, 7 H, $C_6H_5C\equiv$C and C^N^C), 7.54 (d, 8.0 Hz, 2 H, pyridyl of C^N^C), 7.62 (m, 4 H, $C_6H_5C\equiv$C and C^N^C), 7.92 (t, 8.0 Hz, 1 H, pyridyl of C^N^C), 8.04 (dd, 7.4 and 1.0 Hz, 2 H, phenyl of C^N^C). Positive EI-MS: *m*/*z* 527 $[M]^+$. IR (KBr): 2147 cm^{-1} ν(C≡C). Elemental analyses calcd for $C_{25}H_{16}NAu$ (found): C, 56.93 (56.57); H, 3.04 (3.05); N, 2.66 (2.66).

[Au(C^N^C)(C≡CC$_6$H$_5$)] (1) by *Method b*. To a stirred solution of phenylacetylene (0.07 g, 0.65 mmol) in methanol (60 mL) was added sodium hydroxide (0.52 g, 1.30 mmol). The resultant solution was heated at 60 °C for 30 min. [Au(C^N^C)Cl] (0.20 g, 0.43 mmol) was added to the reaction mixture which was then further heated under reflux for 12 h. The mixture was filtered, and the solvent was evaporated to dryness. The product was isolated by column chromatography on silica gel using dichloromethane as eluent. Subsequent recrystallization from slow diffusion of diethyl ether vapor into the concentrated solution gave **1** as pale yellow crystals. Yield: 0.68 g (30%).

[Au(C^N^C)(C≡CC$_6$H$_4$−Cl-*p*)] (2). This was synthesized by *method a* according to a procedure similar to that of **1** except (4-chlorophenyl)acetylene (0.09 g, 0.65 mmol) was used in place of phenylacetylene. Pale yellow crystals of **2** were obtained. Yield: 0.21

(16) (a) Demas, J. N.; Crosby. G. A. *J. Phys. Chem.* **1971**, *75*, 991. (b) van Houten, J.; Watts, R. *J. Am. Chem. Soc.* **1976**, *98*, 4853.
(17) (a) Che, C. M.; Wong. K. Y.; Anson, F. C. *J. Electroanal. Chem. Interfacial Electrochem.* **1987**, *226*, 211. (b) Connelly, N. G.; Geiger, W. E.; *Chem. Rev.* **1996**, *96*, 877.
(18) Written with the cooperation of the program authors Otwinowski, Z., and Minor, W.: Gewirth, D. *DENZO: "The HKL Manuals-A description of programs DENZO, XDISPLAYF, and SCALEPACK"*; Yale University: New Haven, CT, 1995 .
(19) Sir97: a new tool for crystal structure determination and refinement: Altomare, A.; Burla, M. C.; Camalli, M.; Cascarano, G.; Giacovazzo, C.; Guagliardi, A.; Moliterni, A. G. G.; Polidori, G.; Spagna, R. *J. Appl. Crystallogr.* **1998**, *32*, 115.
(20) SHELXL97: Sheldrick, G. M. *SHELXL97: Programs for Crystal Structure Analysis* (release 97-2); University of Göttingen: Göttingen, Germany, 1997.

g (85%). ^{1}H NMR (300 MHz, CD_2Cl_2, 298 K, relative to Me_4Si)/ppm: δ 7.25−7.42 (m, 6 H, $-C_6H_4C\equiv C$ and C^N^C), 7.53 (m, 6 H, $-C_6H_4C\equiv C$ and pyridyl of C^N^C), 7.60 (dd, 7.0 and 1.0 Hz, 2 H, phenyl of C^N^C), 7.90 (t, 8.0 Hz, 1 H, pyridyl of C^N^C), 8.00 (dd, 7.2 and 1.0 Hz, 2 H, phenyl of C^N^C). Positive EI-MS: *m*/*z* 562 $[M]^+$. IR (KBr): 2157 cm^{-1} ν(C≡C). Elemental analyses calcd for $C_{25}H_{15}NClAu\cdot{}^1/_2H_2O$ (found): C, 52.59 (52.85); H, 2.80 (2.66); N, 2.45 (2.40).

[Au(C^N^C)(C≡CC$_6$H$_4$−NO$_2$-*p*)] (3). This was synthesized by *method a* according to a procedure similar to that of **1** except (4-nitrophenyl)acetylene (0.10 g, 0.65 mmol) was used in place of phenylacetylene. Yellow crystals of **3** were obtained. Yield: 0.20 g (81%). ^{1}H NMR (400 MHz, CD_2Cl_2, 298 K, relative to Me_4Si)/ppm: δ 7.31 (dt, 7.4 and 1.3 Hz, 2 H, phenyl of C^N^C), 7.42 (dt, 7.4 and 1.3 Hz, 2 H, phenyl of C^N^C), 7.55 (d, 8.0 Hz, 2 H, pyridyl of C^N^C), 7.64 (dd, 7.2 and 1.2 Hz, 2 H, phenyl of C^N^C), 7.73 (d, 9.0 Hz, 2 H, $-C_6H_4C\equiv C$), 7.93 (t, 8.0 Hz, 1 H, pryidyl of C^N^C), 8.00 (dd, 7.2 and 1.2 Hz, 2 H, phenyl of C^N^C), 8.22 (d, 9.0 Hz, 2 H, $-C_6H_4C\equiv C$). Positive EI-MS: *m*/*z* 572 $[M]^+$. IR (KBr): 2146 cm^{-1} ν(C≡C), 1341 and 1588 cm^{-1} ν(N−O). Elemental analyses calcd for $C_{25}H_{15}N_2O_2Au\cdot{}^1/_2H_2O$ (found): C, 51.65 (51.62); H, 2.77 (2.65); N, 4.82 (4.75).

[Au(C^N^C)(C≡CC$_6$H$_4$−OCH$_3$-*p*)] (4). This was synthesized by *method a* according to a procedure similar to that of **1** except (4-methoxyphenyl)acetylene (0.09 g, 0.65 mmol) was used in place of phenylacetylene. Pale yellow crystals of **4** were obtained. Yield: 0.21 g (86%). ^{1}H NMR (400 MHz, CD_2Cl_2, 298 K, relative to Me_4Si)/ppm: δ 3.88 (s, 3 H, OCH_3), 6.91 (d, 8.9 Hz, 2 H, $-C_6H_4C\equiv C$), 7.27 (dt, 7.3 and 1.3 Hz, 2 H, phenyl of C^N^C), 7.40 (dt, 7.3 and 1.3 Hz, 2 H, phenyl of C^N^C), 7.50−7.56 (m, 4 H, pyridyl of C^N^C and $-C_6H_4C\equiv C$), 7.60 (dd, 7.6 and 1.0 Hz, 2 H, phenyl of C^N^C), 7.90 (t, 8.0 Hz, 1 H, pyridyl of C^N^C), 8.02 (dd, 7.6 and 1.0 Hz, 2 H, phenyl of C^N^C). Positive EI-MS: *m*/*z* 557 $[M]^+$. IR (KBr): 2157 cm^{-1} ν(C≡C). Elemental analyses calcd for $C_{26}H_{18}NOAu\cdot{}^1/_2H_2O$ (found): C, 55.12 (55.15); H, 3.36 (3.28); N, 2.47 (2.48).

[Au(C^N^C)(C≡CC$_6$H$_4$−NH$_2$-*p*)] (5). This was synthesized by *method a* according to a procedure similar to that of **1** except (4-aminophenyl)acetylene (0.08 g, 0.65 mmol) was used in place of phenylacetylene. Deep yellow crystals of **5** were obtained. Yield: 0.19 g (80%). ^{1}H NMR (300 MHz, CD_2Cl_2, 298 K, relative to Me_4Si)/ppm: δ 3.84 (s, 2 H, NH_2), 6.67 (d, 8.6 Hz, 2 H, $-C_6H_4C\equiv C$), 7.30 (dt, 7.5 and 1.3 Hz, 2 H, phenyl of C^N^C), 7.39−7.45 (m, 4 H , phenyl of C^N^C and $-C_6H_4C\equiv C$), 7.56 (d, 8.0 Hz, 2 H, pyridyl of C^N^C), 7.65 (dd, 7.4 and 1.0 Hz, 2 H, phenyl of C^N^C), 7.92 (t, 8.0 Hz, 1 H, pyridyl of C^N^C), 8.07 (dd, 7.4 and 1.0 Hz, 2 H, phenyl of C^N^C). Positive EI-MS: *m*/*z* 542 $[M]^+$. IR (KBr): 2143 cm^{-1} ν(C≡C), 3338 and 3421 cm^{-1} ν(N−H). Elemental analyses calcd for $C_{25}H_{17}N_2Au\cdot{}^1/_2H_2O$ (found): C, 54.45 (54.59); H, 3.27 (3.13); N, 5.08 (5.04).

[Au(C^N^C)(C≡CC$_6$H$_4$−C$_6$H$_{13}$-*p*)] (6). This was synthesized by *method a* according to a procedure similar to that of **1** except (4-hexylphenyl)acetylene (0.12 g, 0.65 mmol) was used in place of phenylacetylene. Pale yellow solid of **6** were obtained. Yield: 0.19 g (72%). ^{1}H NMR (300 MHz, CD_2Cl_2, 298 K, relative to Me_4Si)/ppm: δ 0.91 (t, 7.0 Hz, 3 H, $-CH_3$), 1.31−1.39 (m, 6 H, $-CH_2-$), 1.62−1.67 (m, 2 H, $-CH_2-$), 2.64 (t, 7.7 Hz, 2 H, $-CH_2-$), 7.18 (d, 8.3 Hz, 2 H, $-C_6H_4C\equiv C$), 7.25 (dt, 7.4 and 1.3 Hz, 2 H, phenyl of C^N^C), 7.37 (dt, 7.4 and 1.3 Hz, 2 H, phenyl of C^N^C), 7.50 (m, 4 H, pyridyl of C^N^C and $-C_6H_4C\equiv C$), 7.57 (dd, 7.3 and 1.1 Hz, 2 H, phenyl of C^N^C), 7.87 (t, 8.0 Hz, 1 H, pyridyl of C^N^C), 8.00 (dd, 7.3 and 1.1 Hz, 2 H, phenyl of C^N^C). Positive EI-MS: *m*/*z* 611 $[M]^+$. IR (KBr): 2149 cm^{-1} ν(C≡C). Elemental analyses calcd for $C_{31}H_{28}NAu\cdot{}^1/_2H_2O$ (found): C, 59.95 (60.00); H, 4.51 (4.60); N, 2.26 (2.26).

[Au(C^N^C)(C≡CC$_6$H$_{13}$)] (7). This was synthesized by *method a* according to a procedure similar to that of **1** except 1-octyne (0.07 g, 0.65 mmol) was used in place of phenylacetylene. Pale yellow crystals of **7** were obtained. Yield: 0.16 g (68%). ^{1}H NMR (300 MHz, CD_2Cl_2, 298 K, relative to Me_4Si)/ppm: δ 0.95 (t, 7.0 Hz, 3 H, $-CH_3$), 1.37−1.42 (m, 4 H, $-CH_2-$), 1.63−1.72 (m, 4 H, methylene of C_6H_{13}), 2.49 (t, 6.9 Hz, 2 H, $-CH_2-$), 7.28 (dt, 7.3 and 1.3 Hz, 2 H, phenyl of C^N^C), 7.40 (dt, 7.3 and 1.3 Hz, 2 H, phenyl of C^N^C), 7.53 (d, 8.0 Hz, 2 H, pyridyl of C^N^C), 7.62 (dd, 7.2 and 1.2 Hz, 2 H, phenyl of C^N^C), 7.90 (t, 8.0 Hz, 1 H, pyridyl of C^N^C), 7.99 (dd, 7.2 and 1.2 Hz, 2 H, phenyl of C^N^C). Positive FAB-MS: *m*/*z* 536 $[M]^+$. IR (KBr): 2140 cm^{-1} ν(C≡C). Elemental analyses calcd for $C_{25}H_{24}NAu$ (found): C, 56.08 (55.96); H, 4.52 (4.60); N, 2.62 (2.53).

[Au(*t*BuC^N^C*t*Bu)(C≡CC$_6$H$_5$)] (8). This was synthesized by *method a* according to a procedure similar to that of **1** except [Au(*t*BuC^N^C*t*Bu)Cl] (0.20 g, 3.48 mmol) was used in place of [Au(C^N^C)Cl]. Subsequent diffusion of *n*-pentane vapor into the concentrated dichloromethane solution resulted in the formation of deep yellow crystals of **8**. Yield: 0.19 g (85%). ^{1}H NMR (400 MHz, CD_2Cl_2, 298 K, relative to Me_4Si)/ppm: δ 1.39 (s, 18 H, *t*Bu), 7.35 (m, 5 H, $C_6H_5C\equiv C$), 7.46 (d, 8.0 Hz, 2 H, pyridyl of *t*BuC^N^C*t*Bu), 7.56 (d, 8.2 Hz, 2 H, phenyl of *t*BuC^N^C*t*Bu), 7.60 (dd, 8.2 and 2.0 Hz, 2 H, phenyl of *t*BuC^N^C*t*Bu), 7.86 (t, 8.0 Hz, 1 H, pyridyl of *t*BuC^N^C*t*Bu), 8.18 (d, 2.0 Hz, 2 H, phenyl of *t*BuC^N^C*t*Bu). Positive EI-MS: *m*/*z* 640 $[M]^+$. IR (KBr): 2149 (w) cm^{-1} ν(C≡C). Elemental analyses calcd for $C_{33}H_{32}NAu\cdot{}^1/_2H_2O$ (found): C, 61.11 (61.02); H, 5.09 (5.08); N, 2.16 (2.17).

[Au(C^NTol^C)(C≡CC$_6$H$_4$−C$_6$H$_{13}$-*p*)] (9). This was synthesized by *method a* according to a procedure similar to that of **6** except [Au(C^NTol^C)Cl] (0.24 g, 0.43 mmol) was used in place of [Au(C^N^C)Cl]. Yellow crystals of **9** were obtained. Yield: 0.20 g (80%). ^{1}H NMR (300 MHz, CD_2Cl_2, 298 K, relative to Me_4Si)/ppm: δ 0.91 (t, 6.8 Hz, 3 H, $-CH_3$), 1.34 (m, 6 H, $-CH_2-$), 1.62−1.64 (m, 2 H, $-CH_2-$), 2.46 (s, 3 H, CH_3 of tolyl), 2.64 (t, 7.7 Hz, 2 H, $-CH_2-$), 7.17 (d, 8.0 Hz, 2 H, $-C_6H_4C\equiv C$), 7.27 (dt, 7.5 and 1.0 Hz, 2 H, phenyl of C^N(Tol)^C), 7.35−7.40 (m, 4 H, phenyl of C^N(Tol)^C and pyridyl of C^N(Tol)^C), 7.47 (d, 8.0 Hz, 2 H, $-C_6H_4C\equiv C$), 7.66−7.71 (m, 6 H, phenyl of C^N(Tol)^C and tolyl), 8.01 (dd, 7.5 and 1.0 Hz, 2 H, phenyl of C^N(Tol)^C). Positive FAB-MS: *m*/*z* 703 $[M]^+$. IR (KBr): 2142 (w) cm^{-1} ν(C≡C). Elemental analyses calcd for $C_{38}H_{34}NAu$ (found): C, 64.99 (64.74); H, 4.85 (4.87); N, 2.00 (1.92).

Computational Details. Calculations were carried out using Gaussian03 software package.[21] Density functional theory (DFT) at the Becke3LYP (B3LYP) level[22] was used to optimize the singlet ground-state (S_0) geometries of the Au(III) complexes **1**−**5**, **7′**, **8**, and **9′**. Based on the ground-state optimized geometries in the gas phase, a nonequilibrium time-dependent (TDDFT) method[23] at the same level associated with a conductor-like polarizable continuum model (CPCM)[24] was employed to study the nature of singlet−singlet transitions in the absorption spectra of **1**−**5** and **7**−**9** (CH_2Cl_2 as the solvent). The tandem use of CPCM and TDDFT has been found to be a suitable computational approach for the treatment of the solvent effects on the excited-state energies of the transition metal complexes.[25] The unrestricted

(21) Frisch, M. J., et al. *Gaussian 03*, revision C.02; Gaussian, Inc.: Wallingford, CT, 2004 (see Supporting Information for the full author list).
(22) (a) Lee, C.; Yang, W.; Parr, R. G. *Phys. Rev. B* **1988**, *37*, 785. (b) Becke, A. D. *J. Chem. Phys.* **1993**, *98*, 5648. (c) Stephens, P. J.; Devlin, F. J.; Chabalowski, C. F.; Frisch, M. J. *J. Phys. Chem.* **1994**, *98*, 11623.
(23) (a) Stratmann, R. E.; Scuseria, G. E.; Frisch, M. J. *J. Chem. Phys.* **1998**, *109*, 8218. (b) Bauernschmitt, R.; Ahlrichs, R. *Chem. Phys. Lett.* **1996**, *256*, 454. (c) Casida, M. E.; Jamorski, C.; Casida, K. C.; Salahub, D. R. *J. Chem. Phys.* **1998**, *108*, 4439.
(24) (a) Barone, V.; Cossi, M. J. *Phys. Chem. A* **1998**, *102*, 1995. (b) Cossi, M.; Rega, N.; Scalmani, G.; Barone, V. *J. Comput. Chem.* **2003**, *24*, 669.
(25) (a) Villegas, J. M.; Stoyanov, S. R.; Huang, W.; Rillema, D. P. *Inorg. Chem.* **2005**, *44*, 2297. (b) Villegas, J. M.; Stoyanov, S. R.; Huang, W.; Lockyear, L. L.; Reibenspies, J. H.; Rillema, D. P. *Inorg. Chem.* **2004**, *43*, 6383. (c) Stoyanov, S. R.; Villegas, J. M.; Rillema, D. P. *Inorg. Chem. Commun.* **2004**, *7*, 838. (d) Vlček, A., Jr.; Záliš, S. *J. Phys. Chem. A* **2005**, *109*, 2991.
(26) Andrae, D.; Häussermann, U.; Dolg, M.; Stoll, H.; Preuss, H. *Theor. Chim. Acta* **1990**, *77*, 123.
(27) Ehlers, A. W.; Böhme, M.; Dapprich, S.; Gobbi, A.; Höllwarth, A.; Jonas, V.; Köhler, K. F.; Stegmann, R.; Veldkamp, A.; Frenking, G. *Chem. Phys. Lett.* **1993**, *208*, 111.

(U)B3LYP was used to optimize the low-lying triplet states of all the complexes for the investigation of the nature of the emissive states. The calculated emission maxima were estimated from the differences between the triplet- and ground-state energies at their corresponding equilibrium geometries. To account for the solvent effect on the calculated emission energies, single-point CPCM calculations using CH_2Cl_2 as a solvent were performed on gas-phase optimized ground- and triplet excited-state geometries. The Stuttgart effective core potentials (ECPs) and the associated basis set were applied to describe Au[26] with an f polarization function (ζ_f(Au) = 1.050),[27] while, for all other atoms, the 6-31G(d) basis set[28] was used. All the geometry optimizations were carried out with no symmetry constraint. Vibrational frequencies were calculated for all stationary points to verify that each was a minimum (NIMAG = 0) on the potential energy surface.

Acknowledgment. V.W.-W.Y. acknowledges support from the University Development Fund, the URC Seed Funding for Strategic Research Theme on Organic Optoelectronics, and the Faculty Development Fund of The University of Hong Kong, The University of Hong Kong Foundation for Educational Development and Research Limited, and the RGC Central Allocation Vote (HKU 2/05C). The work described in this paper has been supported by a CERG Grant from the Research Grants Council of Hong Kong Special Administrative Region, China (Project No. HKU 7049/05P). L.-L.H. acknowledges the receipt of a postgraduate studentship, and W.H.L. the receipt of a University Postdoctoral Fellowship, both from The University of Hong Kong. We also thank Professor Zhenyang Lin from the Hong Kong University of Science and Technology for his helpful discussions on the theoretical studies and the Computer Center at The University of Hong Kong for providing the computational resources.

(28) (a) Hehre, W. J.; Ditchfield, R.; Pople, J. A. *J. Chem. Phys.* **1972**, *56*, 2257. (b) Hariharan, P. C.; Pople, J. A. *Theor. Chim. Acta* **1973**, *28*, 213. (c) Francl, M. M.; Pietro, W. J.; Hehre, W. J.; Binkley, J. S.; Gordon, M. S.; Defrees, D. J.; Pople, J. A. *J. Chem. Phys.* **1982**, *77*, 3654.

Note Added after Print Publication. Due to a production error, some of the subscript notation did not appear properly in the Computational Studies section, including Tables 6 and 7, in the version of this article published on the Web on March 16, 2007 (ASAP), and in the April 11, 2007 issue (Vol. 129, No. 14, pp 4345−4365). The corrected electronic versions were published on August 28, 2007, and an Addition and Correction appears in the September 19, 2007 issue (Vol. 129, No. 37).

Supporting Information Available: Selected structural parameters of the coplanar forms, TDDFT/CPCM orbital and excitation energies, % composition of selected MOs, (U)B3LYP electronic energies, Cartesian coordinates of optimized structures, singly occupied orbitals of the optimized triplet state in **1** and **5**, crystallographic data for **1**−**5** and **7**−**9**, and complete ref 21. This material is available free of charge via the Internet at http://pubs.acs.org.

JA068264U